ADSORPTIVE REMOVAL OF NORFLOXACIN FROM AQUEOUS SOLUTION BY REDUCED GRAPHENE OXIDE ANCHORED COPPER FERRITE COMPOSITE

A thesis submitted towards the partial fulfilment of the Masters of Engineering degree in Chemical Engineering

By

ADITYA SAHA

Class Rol No.: 002110302006

Exam Roll No. : M4CHE23001

Registration No. : 160018 of 2021-2022

Under the guidance of

Dr. SASWATA BOSE

&

Dr. MEHABUB RAHAMAN

Department of Chemical Engineering

Jadavpur University

Kolkata – 700032

DECLARATION OF ORIGINALITY AND COMPLIANCE WITH ACADEMIC ETHICS

I hereby declare that this thesis contains a literature survey and original research work by the undersigned candidate, as part of his "***Master of Engineering in Chemical Engineering***" study. All information in this document has been obtained and presented following academic rules and ethical conduct.

I also declare that, as required by these rules and conduct, I have fully cited and referenced all materials and results that are not original to the research work.

Name: **ADITYA SAHA**

Registration Number: **160018 of 2021-2022**

Thesis Title: **"ADSORPTIVE REMOVAL OF NORFLOXACIN FROM AQUEOUS SOLUTION BY REDUCED GRAPHENE OXIDE ANCHORED COPPER FERRITE COMPOSITE"**

Signature:

CERTIFICATION

This is to certify that **Aditya Saha**, a final year student in the Master of Engineering examination in the Department of Chemical Engineering, Jadavpur University, bearing Registration No.: 160018 has completed the thesis work entitled **"ADSORPTIVE REMOVAL OF NORFLOXACIN FROM AQUEOUS SOLUTION BY REDUCED GRAPHENE OXIDE ANCHORED COPPER FERRITE COMPOSITE"** under the guidance of **Dr. Saswata Bose** and **Dr. Mehabub Rahaman** during his course curriculum. This work has not been reported earlier anywhere and can be approved for submission in partial fulfilment of the Master of Engineering in Chemical Engineering.

Dr. Saswata Bose
Assistant Professor
Chemical Engg. Dept. JU

Dr. Mehabub Rahaman
Assistant Professor
Chemical Engg. Dept. JU

Dr. Rajat Chakraborty
Head of the Department
Chemical Engg. Dept. JU

Dean
Faculty of Engineering and Technology, JU

CERTIFICATE OF APPROVAL

This thesis is hereby approved as a creditable study of an engineering subject carried out and presented in a manner satisfactory to warrant its acceptance as a prerequisite to the degree for which it has been submitted. It is understood by this approval that the undersigned don't endorse or approve any statement made, opinion expressed or conclusion drawn therein but approve the thesis only for which it is submitted.

_____

Aditya Saha

M.E. Exam Roll No. M4CHE23001

Chemical Engg. Dept. JU

ACKNOWLEDGEMENT

Though the following project is individual project work, I would never be successful in smoothly completing my project without help, guidance, assistance and inspiration from a lot of people. At the start of this report, I would like to thank all those persons who have helped me in this endeavour. Without their guidance and help it would not be possible for me to progress and plan about this project.

I would sincerely express my gratitude towards my guide **Dr. Saswata Bose** and **Dr. Mehabub Rahaman** for their valuable guidance and cooperation and for providing me with the opportunity to accomplish the project. Without their guidance and assistance, I would never be able to work successfully in this area. I am greatly thankful to them for guiding me always throughout my project work.

I would like to thank my lab mate who consistently helped me while performing and planning this project.

I would also like to express gratitude to the HOD and all faculties of the Chemical Engineering Department at Jadavpur University.

Thanking You,

Aditya Saha

Class Roll No.: 002110302006

Exam Roll No.: M4CHE23001

Registration No.: 160018 of 2021-22

M.E. 2nd Year

ABSTRACT

Unrestricted discharge of pharmaceuticals and their waste in the surrounding and the contamination of the aquatic environment are one of the burning topics in pollution-removing research works. In this research paper adsorption method is employed for which a novel adsorbent reduced graphene oxide based copper ferrite is prepared by wet method to remove Norfloxacin which is 3rd generation antibiotic and also found in the environment in significant amounts from aqueous solution. The SEM micrograph demonstrates that copper ferrite was successfully deposited on the reduced graphene oxide flakes. The EDS result demonstrates the presence of copper and iron metal in the adsorbent. The maximal reduction of graphene oxide into reduced graphene oxide has been detected using XRD data. The XRD examination of copper ferrite has proven that $CuFe_2O_4$ and a trace amount of CuO were formed. According to the FTIR analysis, as graphene oxide reduces to form reduced graphene oxide, fewer oxygen-containing functional groups are present. BET analysis was done to find out the pore volume and surface area of the adsorbent. The highest removal efficiency was found to be 90.55%. The process followed the Langmuir isotherm which gives the maximum adsorption capacity of 296.74 $mg.g^{-1}$. Pseudo-second-order kinetics was best fitted for the process. After 5 cycles of regeneration of the adsorbent, a minor drop in removal efficiency was observed.

TABLE OF CONTENT

LIST OF FIGURES

LIST OF TABLES

LIST OF ABBREVIATIONS

NOR = Norfloxacin

GO = Graphene Oxide

rGO = Reduced Graphene Oxide

HRG = Highly Reduced Graphene Oxide

SF = Spinal Ferrite

CF = Copper Ferrite

rGOCF = Reduced Graphene Oxide-Based Copper Ferrite

SEM = Scanning Electron Microscope

EDS = Energy Dispersive X-Ray Spectroscopy

XRD = X-Ray Diffraction

FTIR = Fourier Transform Infrared Ray

BET = Brunauer-Emmett-Teller

BJH = Barrett–Joyner–Halenda

CHAPTER 1: INTRODUCTION

1.1 OVERVIEW

The most crucial element for any living thing to survive is regarded to be water. Water is accessible in large quantities, but it is seriously contaminated in terms of quality. As a result, the gap between the availability and demand of usable water widens daily. The activities and measures necessary to handle waste from its creation to its disposal are referred to as waste management. This covers garbage collection, transportation, treatment, and disposal, as well as the oversight and control of the waste management procedure. The process of removing pollutants from water effluent and releasing them into the environment is known as wastewater treatment. If not, it will harm water systems and harm aquatic life. Approximately 52% of wastewater is cleaned globally.

Pharmaceutical wastes from the manufacturing industries and municipal waste are also contaminating the drinking water. Some pharmaceuticals like acetaminophen, codeine, caffeine, pesticides, trihalomethane etc. are detected at more than or equal to the detection limit which is also a wake-up call to manage this problem with greater significance.[1]

Discharge from the hospital and animal veterinary, municipal sewage water, use of contaminated manure in agriculture and washed-off unabsorbed beauty and personal care products are the main sources from where the active form of antibiotics is encountered.

There are no strict regulations on how to monitor the concentration of antibiotics in the environment, investigate the environmental effect of these compounds and evaluate the environmental risk of antibiotics globally concerning soil, underground waters, and wastewater contamination. The lack of agreement regarding the safe environmental concentrations of antibiotic residues in terms of the development of resistance and the dearth of convincing scientific evidence regarding environmental pollution with drug residues may help to explain this legislative laxity and the absence of specific regulations.[2]

India and China are the two largest producers of pharmaceuticals but there are no definite regulations or suggested guidelines for the pharmaceutical waste discharged into the environment[3]. Many countries like Germany and Norway in European Union are also rising the issue of imposing strict guidelines for the pharmaceutical industries on the legislative authorities[4]. According to the Environment Protection Agency Report (2015), the USA has considered eight pharmaceutical products as hazardous waste.

An antibiotic is one kind of medicine that is generally used in the fight against bacterial infection and for the growth of livestock. Reports show that the consumption of antibiotics is much higher in animal husbandry compared to human medicine consumption. Van Boeckel et al. published the global footprint of antibiotic consumption in livestock. It shows that in the year 2010, antibiotic consumption was 63,151 tons and it will rise to 67% within the year 2030. In BRICS nations the figure is very alarming[5], [6].

Antibiotics are made to stop harmful bacteria from growing on people or other animals. However, it has been discovered that antibiotics may have adverse effects on the microbial community and the microbial processes that occur in the environment, such as inhibiting bacterial growth, affecting bacterial diversity, lowering the ratio of bacteria to fungi, decreasing functional diversity, reducing nitrification and denitrification, blocking iron reduction, and affecting arsenate reduction.

Norfloxacin ($C_{16}H_{18}FN_3O_3$), a fluoroquinolone antibiotic with a broad range, can prevent DNA helicase activity during DNA replication and hinder cell division, both of which can kill bacteria. It has been magnetization that fluoroquinolones harm the microbial population by changing the variety and composition of bacteria, for example. Additionally, quinolones can form complexes with a range of metal ions, including Ca^{2+}, Mg^{2+}, Fe^{3+} and Al^{3+} resulting in environmental stability over the long term. According to reports, norfloxacin concentrations in polluted soil may reach up to 9.8 mg/kg, and in sewage and surface water, they can reach up to 6.8 μg/L. Norfloxacin is also one of the antibiotics that are mostly found in the sediment, with values reaching 6.5-2616.0 mg/kg.[7]

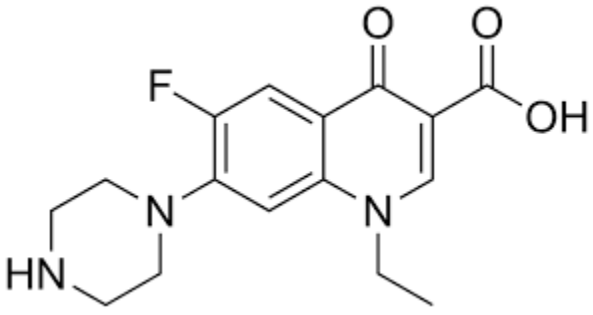

Figure 1: Chemical Structure of NOR

So, one of the alarming concerns about environmental pollution control is to eliminate pharmaceutical waste from mainly aquatic environments as well as from the surface. Conventional

wastewater treatment plants (WWTP) cannot work with 100% efficiency. Sludge and effluents that come out from these plants contain antibiotics and sometimes the sludge is used as manure in the agricultural field and the effluent is discharged into the environment[8].

Many advanced physicochemical and biological processes are now applied to remove pharmaceutical waste from water bodies. Some of them are described below,

- Coagulation & Sedimentation: The process of coagulation creates a gelatinous material to capture the wastewater's charged particles and magnetization their charges. This builds into a bulk that can settle. Aluminium sulphate is used to treat wastewater with a high pH, whereas sodium aluminate is used to treat drinking water. Rapid mixing is used to distribute the coagulant evenly. This technique can get rid of hazardous organic material, suspended solids, and more. The enormous mass created during the coagulation phase settles down during the sedimentation process because it has a higher density than water and falls as a result of gravity. This method's primary flaw is its inability to remove dissolved organic materials.
- Advanced Oxidation Process (AOP): In this process, the pollutants form free radicals by oxidizing through the different advance oxidizing agent. Some of the most used advanced oxidation processes are Wet Air Oxidation (WAO), Ozonation, Fenton Reaction, Photocatalytic Oxidation etc.
  - The WAO process is first introduced in the paper and pulp industry to eliminate black liquor from the effluent. The main oxidizing agent used in this process is oxygen. Oxygen turns the organic matter into small inorganic molecules at high temperatures and pressure. The efficiency of this process in COD removal is 90%.
  - In the ozonation process, ozone is used as an oxidizing agent. This process is very efficient in wastewater treatment.
  - The Fenton process is generally carried out at normal temperatures and pressure, but there is a high chance of oxidant loss for the decomposition of H_2O_2.
  - Photocatalytic oxidation is the combination of UV-ray and oxidant in which the exciting UV-ray decomposes the oxidant and produces a more strong free radical oxidant which can decompose refractory organic pollutants.

- Membrane Separation: Under certain driving forces across the membrane, the water permeates through the membrane selectively. There are many kinds of membrane separation processes. Some of them are discussed below.
  - Microfiltration is a process where static pressure is the driving force and is performed by sieve separation of the membrane.
  - Ultrafiltration works under pressure difference driving force and the macromolecules and colloids are removed.
  - Reverse Osmosis is the process to separate the inorganic salts from the water. But this process requires pretreatment.
- Adsorption: This is one of the easiest operations in wastewater treatment and the recovery of adsorbent is very important. Low energy consumption, flexible and simple design and environment friendly are the main advantages of this process.[9]

1.2 ADSORPTION

Adsorption is a surface phenomenon where mass transfer takes place from the bulk phase to the adsorbent surface. Adsorption is associated with two types of attraction forces namely Physisorption and Chemisorption. In the 1st case, Van-Der Waal's force helps to attract adsorbate molecules to the surface. In the latter case, the presence of functional groups on the adsorbent surface leads to the formation of a chemical bond with the adsorbate molecule. There are three steps in the adsorption process. In the first step, the adsorbate molecules diffuse from the bulk phase to the solid-fluid external interphase. This is known as film diffusion. In the second step, the molecules diffuse into the pores known as particle diffusion. In the third phase, the adsorption occurs on the adsorbent surface.

The relationship between the adsorbate in the liquid phase and the adsorbate adsorbed on the adsorbent surface at equilibrium at constant temperature in known as adsorption isotherm. Following is the adsorption isotherm equation,

$$\frac{\frac{p}{p_0}}{v[1-\left(\frac{p}{p_0}\right)]} = \frac{c-1}{v_m c}\left(\frac{p}{p_0}\right) + \frac{1}{v_m c}$$

Here p and p_0 are the equilibrium and saturation pressure of adsorbate at the temperature of adsorption respectively. v is the adsorbed gas quantity and v_m is the monolayer adsorbed gas

quantity. C is the isotherm constant. Now based on (p/p_0) and c value there are five types of adsorption isotherm available. In the case of type I isotherm is obtained when $P/P_o < 1$ and $c > 1$ in the equation, which is related to the adsorption energy of the first monolayer and varies from solid to solid. The characterization of microporous materials, those with pore diameters less than 2 nm, gives this type of isotherm. While type II isotherm is obtained when $c > 1$ in the equation. This is the most common isotherm obtained when using the BET technique. At very low pressures, the micropores fill with nitrogen gas. At the knee, monolayer formation is beginning and multilayer formation occurs at medium pressure. At higher pressures, capillary condensation occurs. Type III isotherm is obtained when the $c < 1$ and shows the formation of a multilayer. Because there is no asymptote in the curve, no monolayer is formed. Type IV isotherm occurs when capillary condensation occurs. Gases condense in the tiny capillary pores of the solid at pressures below the saturation pressure of the gas. At the lower pressure regions, it shows the formation of a monolayer followed by a formation of multilayers. Surface area characterization of mesoporous materials, with pore diameters between 2 - 50 nm, gives this type of isotherm. Type V isotherm is very much similar to type IV isotherm.

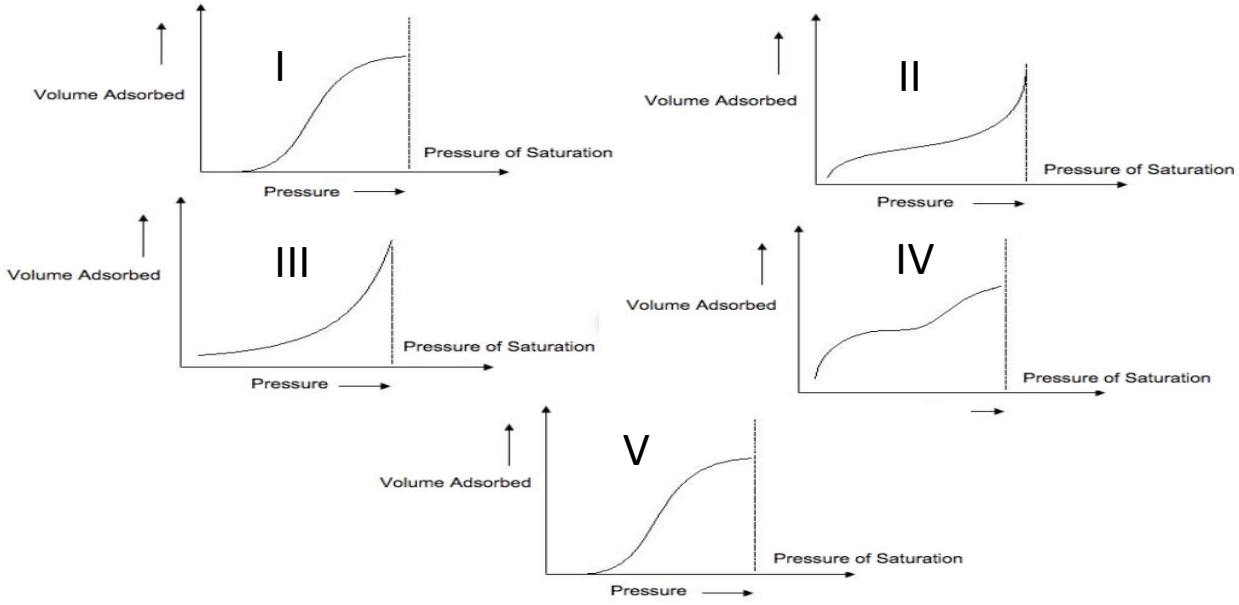

Figure 2: Different Types of Adsorption Isotherm

Over the years, several adsorbents were used in wastewater treatment. Some of them are activated carbon, chitosan, zeolite, silica gel, alumina etc. Activated carbon is very expensive. To reuse, activated carbon needs to be treated with solvent which is also very costly. Alternative methods

like thermal and homogeneous advanced oxidation (UV/H_2O_2 and H_2O_2/O_3) were investigated but the processes are very rare in use. Chitosan displays considerable drawbacks like low adsorption capacity, low surface area and lack of reusability [10]. Zeolite has also some limitations like it is highly sensitive to deactivation by irreversible adsorption or steric blockage of heavy secondary products and the impossibility of using their microporosity for the synthesis of bulky molecules [11]. The main disadvantage of silica gel is the low water exchange due to the high relative pressure required for adsorption and also shows low adsorption capacity [12].

Environmental researchers are currently investigating carbon-based nanomaterial including fullerenes, carbon nanotubes (CNTs) and graphene as adsorbents for water treatment in light of the burgeoning advantages of nanotechnology. Graphene, a 2D sheet of carbon atoms arranged in a hexagonal lattice, is one of the new-generation nanoparticles which can be used as an adsorbent due to its high surface area to mass ratio leading to a great number of adsorption sites along with uniform pore distribution. The surface resistance is also very high. Due to the hexagonal lattice structure, a cloud of delocalized electrons is generated in graphene which interact with other molecules through π-π stacking interaction. The main drawback of using graphene for water treatment is poor water dispersibility. However, the problem pertaining to poor dispersibility can be overcome by surface functionalization. Till date, rGO has been modified using various metal oxides to improve dispersibility aiming at utilizing rGO-based metal oxide composites as effective adsorbents for contaminant removal from water. Zero-valent iron-graphene, magnetic iron oxide-rGO, magnetic rGO, manganese oxide-rGO and other hybrid composites were used to remove radionuclides[13]. rGO-based manganese oxide has a very good ability for adsorption of Cr^{6+} [14]. Metal ion scavenging applications of HRG/MnO_2 composites have been demonstrated by Sreeprasad et al taking Hg(II) as a model pollutant. rGO magnetite has also performed well in adsorption due to its high surface-to-volume ratio, magnetic properties and short diffusion rate [15].

The SFs are highly abundant in nature, low cost and environmentally benign. In recent years, there has been a lot of focus on the structure of SFs because of their chemical and corrosive stability, high specific surface area, high magnetic permeability, tunability in chemical composition and high thermal and mechanical stability. Tunable size, shape and surface adaptability (easily functionalized with multiple ligands), high surface-to-volume ratio and tunable magnetic property

are all SF manufacturing capabilities. These composites are receiving a lot of interest because of the vast range of applications they have in biological sectors, drug delivery, surface-enhanced Raman scattering, catalysis and wastewater treatment. Copper ferrite alone shows very low adsorption capacity. So, the composite of reduced graphene oxide-based spinal ferrite composite is prepared to increase the adsorption capacity.

Most recently, researchers found that Copper-Oxide is an effective adsorbent. Due to its capacity to modify its physical characteristics when subjected to various environmental circumstances, including phase transitions, electrical switching, semiconducting, magnetic, and electrical properties, CF is a desirable spinel ferrite. The formula for $CuFe_2O_4$ is typically $(Cu^{2+})_{1-x}(Fe^{3+})_x[(Cu^{2+})_x(Fe^{3+})_{2-x}]\ O_4^{2-}$ contains oxygen ions at the face of the unit cell with a face-centred cubic structure, with the metal ions outside the square bracket occupying the tetrahedral positions known as the A site and those inside the square bracket occupying the octahedral positions known as the B site. The versatility of $CuFe_2O_4$'s structural morphologies has also made it a significant ferrite[16]–[19].

In the nanoscale, each magnetic NPs behave like a giant paramagnetic atom with a fast response to applied magnetic fields and manifests unique magnetic properties. The major important magnetic properties of NPs are saturation magnetization (M_S), magnetic anisotropy, remnant magnetization (M_r) and coercivity (H_c). The optimum magnetic moment achieved by magnetic NPs in the presence of applied external magnetic field (MF) due to the parallel alignment of unpaired electrons is termed as M_s. While the net residual magnetization of the material left after the removal of the MF due to some unpaired electrons alignments is known as M_r. The resistance of a ferromagnetic material to become magnetization is known as H_c, and it is used to categorise the magnetic into soft and hard magnets.

So, the development of graphene based SF provides a high theoretical surface area of graphene and magnetic property of spinal ferrite which help to adsorb charged particles from the aqueous solution. That is why, reduced graphene oxide anchored CF had been chosen as an adsorbent for this project. Reduced graphene oxide anchored CF can be prepared economically and comfortably in the lab.

Research pertaining to heavy metals and dyes removal employing reduced graphene oxide anchored SF as adsorbent has been adequately addressed [20]–[24] but research aiming at the removal of the pharmaceuticals by the same, has not been reported to date. Therefore, exploring the effectiveness of reduced graphene oxide anchored SF as an adsorbent for the removal of pharmaceuticals from its aqueous solution is of utmost importance.

1.3 RESEARCH OBJECTIVES

There are no strict regulations to impose on the pharmaceutical company also the processes used nowadays are very costly and skilful labour is required which is not affordable for all scales of businesses. That is why the main purpose of this work is to prepare an adsorbent which is low-cost, highly efficient, easy to recover, has a significant surface area, large pore size and is selective to pharmaceuticals.

The objectives of our present work are as follows,

1. Procurement of Graphite powder and preparation of GO by modified Hummer's method.
2. Preparation of rGOCF by hydrothermal synthesis method with the help of hydrated salt of Copper and Iron and with rGO.
3. Study of the effect of the wide range of pH, contact time, initial adsorbate (pharmaceutical) concentration, adsorbent dosage and temperature.
4. Understanding the morphology and micrograph from SEM, metal composition from XRD, and presence of rGO and CF by UV-Vis spectroscopy. The presence of a functional group was confirmed by FTIR. The surface area was found by the BET method.
5. Linear and nonlinear isotherm of Langmuir and Freundlich, and linear isotherm of Temkin were analysed.
6. Pseudo-first-order, pseudo-second-order kinetics and intra-particle diffusion were studied to understand the kinetics of the process.
7. The thermodynamics study was carried out to find out the enthaphy change of the process, spontaneity and randomness of the system.
8. Regeneration Study was carried out to find the reusability efficiency of rGOCF.

CHAPTER 2: LITERATURE REVIEW

2.1 REMOVAL OF POLLUTANTS USING SPINAL FERRITE AS ADSORBENT

Tu YaoJen et al used nano-magnetic $CuFe_2O_4$ to remove Molybdenum from wastewater. Nano-magnetic $CuFe_2O_4$ was prepared from printed circuit board industrial sludge. The maximum adsorbent capacity was found to be 30.58 $mg.g^{-1}$ at pH 2.75. The adsorption process fitted well in the Langmuir adsorption model[25].

Yueming et al reported the use of $MnFe_2O_4$ as an adsorbent for the removal of Pb(II) and Cu(II) from the wastewater. The magnetic porous ferrospinal was prepared by a sol-gel process. The adsorption process followed the pseudo-second-order kinetics and best fitted on the Langmuir isotherm. The adsorption capacity was reported as 69.1 and 60.5 $mg.g^{-1}$ for Pb(II) and Cu(II) respectively[26].

Zhenhu Li et al reported the formation of $Ni_xFe_{3-x}O_4$ by the solvothermal process in mixed solvents of ethylene glycol and water. This hollow nanocrystal can be readily tuned by changing the ratio of Ni and Fe in the precursor. It has been observed that if Ni content (X) increases in the nanocrystal then the adsorption capacity of this adsorbent increases towards organic molecules like congo red. If the Ni content increases from 0.2 to 0.85 the adsorption capacity of the adsorbent towards congo red increases from 263 to 500 $mg.g^{-1}$[27].

Al-Sayed et al worked on a project where they prepared nano-$NiFe_2O_4$ to remove Fe(II) from an aqueous solution. The experiment was performed at 150 rpm. The maximum adsorption capacity was reported as 69.8 $mg.g^{-1}$ when the initial concentration of adsorbate was 250 $mg.lit^{-1}$ at 348K. The process was well described by pseudo-second-order kinetics. Langmuir isotherm was well-fitted with the process[28].

Zhang ShengXiao et al reported that $MnFe_2O_4$ and $CoFe_2O_4$ can be good adsorbents for the removal of arsenite (AsIII) and arsenate (AsV). For $MnFe_2O_4$ the adsorption capacities are 94 and 90 $mg.g^{-1}$ and for $CoFe_2O_4$ the values are 100 and 74 $mg.g^{-1}$ for As(III) and As(V) respectively. The desorption study of $MnFe_2O_4$ showed 80% and 90% desorption of As(III) and As(V) respectively with the help of 0.1 M NaOH solution[29].

Buhe Bateer et al reported $MnFe_2O_4$ as a nanoparticle adsorbent for the adsorption of Pb(II) from synthetic wastewater. In this work, $MnFe_2O_4$ is functionalized by secondary surfactants such as

cetyltrimethylammonium bromide(CTAB), sodium dodecyl benzene sulfonate (SDBS) and sodium dodecyl sulfate (SDS). The functionalized nanoparticles show great stability in water which is compatible with Pb (II)adsorption.The adsorption capacities of CTAB, SDBS and SDS stabilized $MnFe_2O_4$ NPs and bare $MnFe_2O_4$ NPs for Pb(II) are respectively 89.55%, 75.05%, 66.07% and 35.2%[30].

Yao-Jen Tu et al prepared $CuFe_2O_4$ from industrial sludge by the combination of acid leaching, chemical exchange and ferrite process. It can remove Cd from aqueous solution at pH 6. The highest removal percentage is 99.9 at the contact time of 30 min and 318K. The maximum adsorption capacity is 17.54 $mg.g^{-1}$. The adsorption process follows pseudo-second-order kinetics and best fits in the Langmuir Isotherm. The SEM image morphology indicated the primary adsorbent particle size ranges from about 20 to 90 nm[31].

Weiling Sun et al reported $CoFe_2O_4$ as an adsorbent for the adsorption of Selenium (Se(IV) and Se(VI)). The maximum adsorption capacities of this nanoparticle are 11.6 and 5.55 $mg.g^{-1}$ for Se(IV) and Se(VI) respectively. The size of the nanoparticle ranges from 10 to 20 nm. Also, this adsorbent showed better adsorption results compare to $MnFe_2O_4$. The adsorption process followed pseudo-second-order kinetics and the Freundlich isotherm fitted best for the adsorption. It is also shown that after the adsorption of Se(IV), the pH_{PZC} shifted from 8 to 5. After the adsorption of Se(VI) the surface of the adsorbent decreased especially pH lower than pH_{PZC}[32].

Zeng SuYuan et al prepared magnetically separable $Ni_{0.6}Fe_{2.4}O_4$ in two steps incorporating a micro-emulsion synthetic process and followed by calcination of the precursor. The adsorbent has a surface area of 113.95 $m^2.g^{-1}$ and a pore diameter of 5.86 nm. The adsorbent is used for the adsorption of congo red (CR) dye. The maximum adsorption capacity is 72.73 $mg.g^{-1}$ and the removal percentage is 92.04. The process followed pseudo-second-order kinetics and the Langmuir isotherm fitted best for the adsorption[33].

Lijun Yang et al prepared magnetic $MnFe_2O_4$ by co-precipitation method to compare the removal of methylene blue (MB) and CR dye from an aqueous solution. The process rate was higher for MB as it reached the equilibrium in a short time compared to CR. In both cases, the process followed pseudo-second-order kinetics. The adsorption of CR best fitted in Langmuir isotherm but the MB fitted well in Freundlich isotherm[34].

Jing Feng et al prepared magnetic ZnO/$ZnFe_2O_4$ by microwave combustion method using NaAc as fuel. The adsorbent showed a larger BET surface area and smaller size with an increase in NaAc dosage. MB as an adsorbate The highest removal recorded at pH 7 was 90% and the adsorption capacity was 37.27 $mg.g^{-1}$. Pseudo-second-order kinetics and Langmuir isotherm were followed. From this project, it can be concluded that fuel content has a significant influence on the morphologies and the adsorption capacity [35].

Rongcheng Wu et al prepared $CuFe_2O_4$ powder for the removal of azo-dye Acid Red B (AR B) from an aqueous solution. It showed good removal at pH<5.5. The maximum adsorption capacity was 86.8 $mg.g^{-1}$. Langmuir isotherm fitted well with this process. The BET surface area was recorded as 88.6 $m^2.g^{-1}$ whereas the average pore diameter and pore volume were 7.02 nm and 0.14 $cm^3.g^{-1}$ [36].

M.A.Rehman et al prepared $CuFe_2O_4$ by micro-emulsion process. This is used for the adsorption of fluoride. The surface area attained was 70 $m^2.g^{-1}$. The size of the nanoparticles is 72 nm[37].

Yao-Jen Tu et al found that phosphorus is an element which critical element due to eutrophication but is also a vital nutrient for the organism in a broad ecosystem. So removing and removal of P from water bodies is very essential. That is why the authors prepare the nano bimetal ferrite $CuFe_2O_4$ by industrial sludge process. The result shows that the removal percentage increases from 9.9 to 99.9 when the value of pH is reduced from 9.06 to 2.64. At pH 2.64 the maximum adsorption capacity was 13.5 $mg.g^{-1}$. The process preferred pseudo-second-order kinetics and fitted well in the Langmuir isotherm [38].

Entesar Al-Hetlani et al prepared activated carbon modified with $CoFe_2O_4$ was prepared as a magnetic adsorbent for the removal of promazine drug from wastewater. The process followed pseudo-second-order kinetics and the maximum adsorption capacity was achieved at Langmuir isotherm which was 90.91 $mg.g^{-1}$. The same adsorbent was tested for the removal of diclofenac and the removal percentage was 84.4 [39].

Zhigang Jia et al prepared mesoporous rodlike $NiFe_2O_4$ by thermal decomposition. Phosphate was used as adsorbate. The process followed Langmuir isotherm with a maximum adsorption capacity of 39.3 $mg.g^{-1}$. Pseudo-second-order kinetics was followed. The mesoporous nickel ferrite demonstrates good adsorption capacity and selective-

ity for phosphate from the mixed $Cr_2O_7^{2-}$, NO^{3-}, SO_4^{2-}, CO_3^{2-} and $S_2O_3^{2-}$ solutions[40].

2.2 REMOVAL OF POLLUTANTS USING GRAPHENE-BASED COMPOSITE AS ADSORBENT

F. A. Jumeri et al synthesized magnetic $ZnFe_2O_4$-rGO nano-composite by microwave method. The authors carried out the batch adsorption process with MB as adsorbate. After 2 hours of adsorption, the removal percentage was 82. The regeneration study showed significant removal in up to 3 cycles. This nano-composite is also used as a photocatalyst [41].

FerdosKordMostafapour et al prepared reduced graphene oxide modified with ammonium ferrous sulfate to make it a magnetic adsorbent to remove amoxicillin from the aqueous solution. At pH 3 the adsorbent showed the highest adsorption capacity which is 98.41 $mg.g^{-1}$. The result was attained at 75 min. But the removal efficiency decreased when the temperature is increased [42].

P. Banerjee et al prepared graphene oxide nanoparticles by Hummer's method for the adsorption of ibuprofen. After 60 min of adsorption, the removal efficiency was 98.17% at pH 6. Though the process reached equilibrium at 180 min. The process followed pseudo-second-order kinetics and fitted well in Langmuir isotherm. The highest adsorption capacity was 3.72 $mg.g^{-1}$ [43].

M. Verma et al prepared rGO base $MnFe_2O_4$ for the adsorption of heavy metal Pb from the aqueous solution. At first, the GO was prepared by Modified Hummer's method. Then the rGO-based $MnFe_2O_4$ was prepared by hydrothermal method. In this process, the highest removal is achieved at pH 6. The process attained 98% removal efficiency within the first 10 min. The process fitted well in Langmuir isotherm. The process followed pseudo-second-order kinetics [44].

Jie Ma et al prepared 3D porous graphene hydrogel (GH) by hydrothermal reduction method. Ciprofloxacin is used as an adsorbent. It is found that GH granules had a higher adsorption rate than GH blocks. The process fitted well with Langmuir isotherm with a maximum adsorption capacity of 235.6 $mg.g^{-1}$. Both the GH granules and GH blocks both followed Boyd model kinetics. At pH 8 the adsorbent shows the highest removal efficiency. There are various adsorption

interaction mechanisms written in this project which are π-π interaction, hydrogen bonding and hydrophobic interaction [45].

Fei Wang et al prepared novel magnetic chitosan grafted graphene oxide for the adsorption of ciprofloxacin. The adsorption process followed pseudo-second-order kinetics. Both Langmuir and Freundlich's isotherm well fitted into this process. The removal efficiency decreased at pH 7 and 9. The regeneration study was carried out up to 4 adsorption cycles where the removal efficiency decreased by up to 72%. Electrostatic interaction and π-π electron interaction were mentioned as the adsorption mechanism [46].

Hossein Mahmood et al prepared graphene oxide-chitosan hydrogel for the removal of diclofenac from the aqueous solution. The optimal ratio of GO and chitosan taken was 2:5. At the pH of 5 the GO-chitosan hydrogel showed an adsorption efficiency of 90.42%. The Langmuir isotherm model was the best-fit model for this process. The process followed pseudo-second-order kinetics. The regeneration study was carried out 5 times but after the 3rd cycle there was a significant drop in adsorption efficiency was shown [47].

Gessica Wernka et al prepared to GO by Modified Hummer's method for the removal of cephalexin from the aqueous solution. The highest removal efficiency was achieved between the pH range of 3 and 6. The adsorption kinetics study revealed that the process followed pseudo-second-order kinetics. The adsorption process reached equilibrium after 7 hrs of adsorption. The Langmuir isotherm fitted well in this process with 164 $mg.g^{-1}$ as the maximum adsorption capacity [48].

Anurag Jaswal et al prepared an rGO-based MoS_2 heterostructure adsorbent for the removal of ofloxacin from the aqueous solution. Though the adsorbent had a very low surface area of 17.17 $m^2.g^{-1}$, the adsorbent showed good removal efficiency and reached equilibrium in 4 hours. The adsorbent regeneration study showed that the adsorbent is stable for the adsorption process of up to 5 cycles. At pH 6 it shows higher removal efficiency of 88%. The process is best fitted with the Langmuir isotherm with a maximum adsorption capacity of 37.31 $mg.g^{-1}$ [49].

From the literature review and the below mentioned comparison study (Table 1) it can be concluded that rGO anchored CF is completely new in case of pharmaceutical adsorption from water.

Table 1: Comparison Study

Adsorbent	Pharmaceutical Pollutant	Initial Pollutant Concentration (ppm)	Maximum Adsorption Capacity ($mg.g^{-1}$)	Reference
rGO modified with Ammonium Ferrous sulfate	Amoxicillin	50	98.41	[39]
rGO	Ibuprofen	6	3.72	[43]
3D porous Graphene Hydrogel	Ciprofloxacin	50	235.6	[45]
Magnetic Chitosan grafted GO	Ciprofloxacin	20	282.9	[46]
GO- Chitosan Hydrogel	Diclofenac	100	132.11	[47]
rGO	Cephalexin	20	164	[48]
rGO based MoS_2Heterosturcture	Ofloxacin	10	37.31	[49]
GO	Aspirin & Acetaminophen	40	61.73 & 20.41	[50]
Graphene Nano Crystalline	Aspirin & Acetaminophen	40	99 & 76.24	[50]
GO	Enrofloxacin	10	45.03	[51]
Maltodextrin-rGO	diclofenac	20	107.90	[52]
Maltodextrin-rGO	Amoxiciline	30	138.3	[52]
rGO based Copper Ferrite	**Norfloxacin**	**90**	**296.7**	**This Study**

CHAPTER 3: MATERIALS & METHODS

3.1 MATERIALS

All chemical reagents were of analytical grade and were used without further purification. Fine graphite powder (98%) was used along with concentrated (about 98%) Sulphuric acid (H_2SO_4) and Potassium Permanganate ($KMnO_4$) purchased from Merck, India. Hydrogen Peroxide (H_2O_2 about 30%), Hydrochloric Acid (HCl about 37%), Copper Nitrate Trihydrate [$Cu(NO_3)_2.3H_2O$], Ferric Nitrate Nonahydrate [$Fe(NO_3)_3.9H_2O$] and Ethanol were procured from Merck, India. Sodium Hydroxide Pellet used to maintain the pH was purchased from Merck, India. Distilled water was used for every batch experiment and washing. Norflox Eye/Ear Drop consists of 0.3% w/v Norfloxacin (NOR) and was purchased from the medical store.

3.2 METHODS

3.2.1 GO Synthesis:

GO was synthesized by modified Hummer's method[53]. At first, 2 g of fine graphite powder (98%) was mixed with 46 ml of 98% concentrated H_2SO_4 and stirred for 30 mins. Since it was an exothermic reaction, an ice bath was used to minimize the heat evolution. Then 6 g of $KMnO_4$ was added very slowly to the mixture and stirred vigorously for 6 hours. The colour of the solution was changed to deep green. Then the deep green reaction mixture was kept in a petri dish at room temperature to cool down. After cooling down, the mixture was added with the proper precaution to 92 ml of distilled water with continuous agitation. The colour of the mixture changed into a deep brown. Then the mixture was stirred for another 2 hours and then poured into 280 ml of distilled water. 30% H_2O_2 was added dropwise to eliminate the excess $KMnO_4$.The colour was changed from deep brown to yellowish brown. Then 5% HCl was added to the mixture to remove any metal impurities. Distilled water was used to wash the product and to bring the pH to 7. Then the product was dried in a hot air oven at 70^0 for 24 hours.

3.2.2 rGO Synthesis:

At first, 106.25 mg GO was dispersed into 80 ml of ethanol and sonicated for 30 mins. Then 6 (M) aqueous solution of NaOH was added dropwise into the above solution to increase the pH to 10 under vigorous stirring and stirred for another 30 mins. The mixture was poured into the teflon-lined autoclave and heated at 150^0C for 24 hours in a hot air oven. Then the autoclave was kept at room temperature for cooling down. Then the mixture was washed with water in a vacuum filter to bring the pH to 7. Then the residue was dried at 60^0C for 24 hours to remove the moisture.

3.2.3 CF Synthesis:

Hydrated salts of copper and iron were used in this process. 4.3 g of $Fe(NO_3)_3.9H_2O$ and 1.3 g of $Cu(NO_3)_2.3H_2O$ were added into 80 ml of ethanol and stirred for 30 mins. Then 6 (M) aqueous solution of NaOH was added dropwise into the above solution to increase the pH to 10 under vigorous stirring and stirred for another 30 mins. The mixture was poured into the teflon-lined autoclave and heated at 150^0C for 24 hours in a hot air oven. Then the autoclave was kept at room temperature for cooling down. Then the mixture was washed with water in a vacuum filter to bring the pH to 7. Then the residue was dried at 60^0C for 24 hours to remove the moisture.

3.2.4 rGOCF Synthesis:

The rGOCF was also prepared by hydrothermal process[54]. 85 mg GO was dispersed into the ethanol and sonicated for 30 mins to increase the surface area. 862 mg of $Fe(NO_3)_3.9H_2O$ and 258 mg of $Cu(NO_3)_2.3H_2O$ were added into 16 ml of ethanol and stirred for 30 min. After this, the above two mixtures were added and stirred for another 30 min at room temperature. Then the pH of the mixture was increased to 10 by adding 6(M) NaOH dropwise and then stirred vigorously for 30 mins. Now the mixture was transferred into the autoclave and heated to 150^0C for 24 hours. The yield was then washed with distilled water in a vacuum filter and dried at 60^0C in a hot air oven for 24 hours.

The preparation process of rGOCF is mentioned in the following schematic:

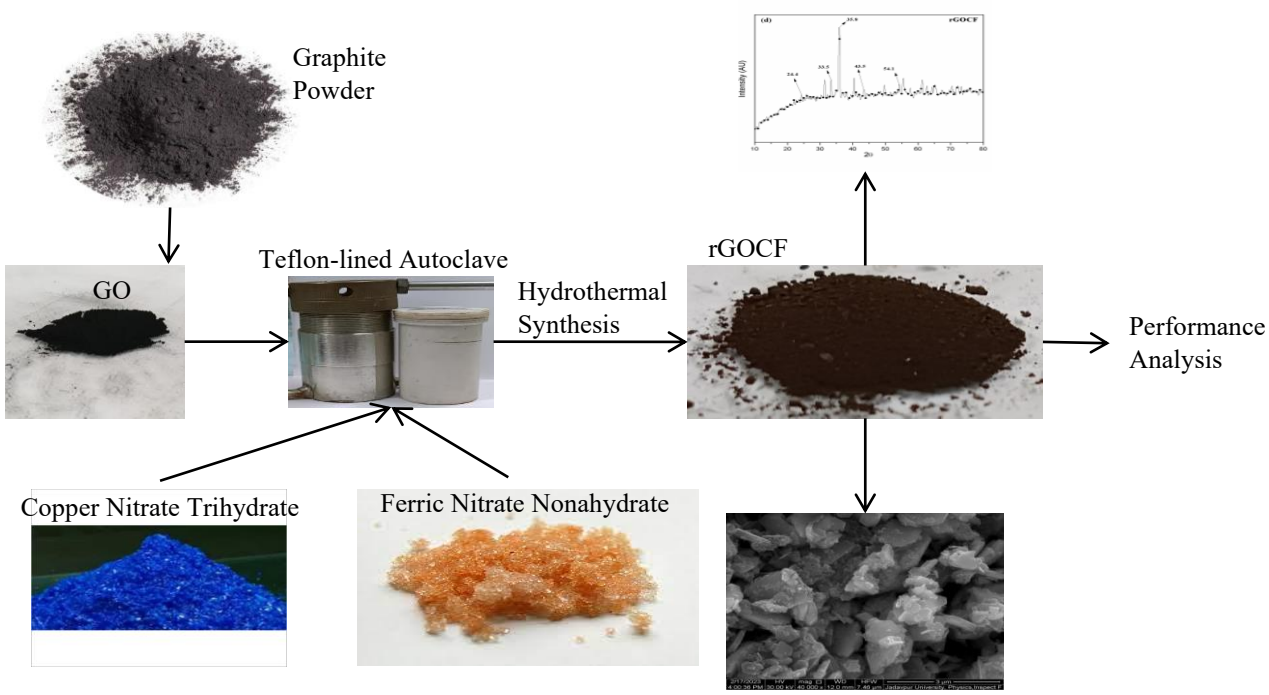

3.2.5 Batch Study:

The Calibration Curve of NOR was prepared at different concentrations and the corresponding absorbance was measured from Perkin Elmar L650 UV-Vis Spectrophotoscopy. The batch experiments of adsorption were carried out in conical flasks by adding a particular amount of water measured in a measuring cylinder and NOR measured by a micro pipet. After that, the adsorbent was measured in a weighing machine precisely and added to the NOR aqueous solution. The adsorption process is carried out in an incubator shaker with a shaking speed of 150 rpm. This is done to find out the effect of different parameters like the pH of the experiment environment, initial concentration of the adsorbate, adsorbent dosage and contact time. Langmuir and Freundlich isotherm (both linear and non-linear model) was studied. Pseudo-1st and 2nd-order kinetics were studied to find out the kinetics of the experiment. A regeneration study was also performed to study the reusability of the adsorbent.

There are two important quantities which are needed to calculate to understand the adsorption isotherm, adsorption kinetics and the effect of different parameters like pH, contact time, adsorbent dosage and initial NOR concentration.

Removal percentage is the quantity which is needed to measure how much NOR is adsorbed compared to the initial concentration of the NOR. The mathematical formula for this is as followed,

$$\%R = \left[\frac{C_0 - C_i}{C_0}\right] * 100$$

Here, C_o and C_i are the concentration of adsorbate (mg.L^{-}1) initially and after time t respectively.

The other quantity is adsorption capacity. This quantity reveals the amount of adsorbent required to adsorb a particular amount of adsorbate (mg.g^{-1}). The mathematical formula is,

$$Q_m = (C_0 - C_i) * \frac{V}{m}$$

Here, V is the volume of adsorbate aqueous solution (ml) and m is the mass of the adsorbent used in the batch adsorption process (mg).

3.2.6 Characterization:

The UV-Vis spectroscopy of the adsorbent was done by Perkin Elmar L650 UV-Vis Spectrophotoscopy by sonicating the adsorbent rGOCF in distilled water for 20 minutes to obtain a homogeneous suspension. The scanning interval was 1 nm and the scanning rate was 200 nm/min. XRD was done by Rigaku Ultima III X-Ray Diffractometer to prepare the diffractometer pattern. The wavelength was set at 1.54 Å. The analysis was conducted at 40 KV voltage and 30 mA current. SEM was done to understand the surface morphology of the adsorbent. Energy-Dispersive X-ray spectroscopy (EDS) was based on the carbon scale. The accelerating voltage for the analysis was 30KV and the working distance was 3 and 5 μm. FTIR was done by JASCO Analyser to find out the functional group present on the surface of the adsorbent. BET surface area analysis was performed in Qunatachrome Autosorb iQ2 Analyser (100-240V, 50/60Hz) to calculate the surface area and pore volume of the sample.

CHAPTER 4: RESULTS & DISCUSSION

4.1 CHARACTERIZATION

4.1.1 SEM Micrograph and EDS Mapping:

The morphology and microstructure of the as-prepared rGOCF were characterized by scanning electron microscope (SEM). The rGO flakes are distinctly visible in the micrograph. The CF particles are well distributed over the framework. The pores are also clearly visible which plays a pivotal role in the adsorption. Overall the SEM micrograph confirms the successful preparation of rGOCF by hydrothermal process. The EDS mapping shows the presence of carbon, oxygen, iron and copper.

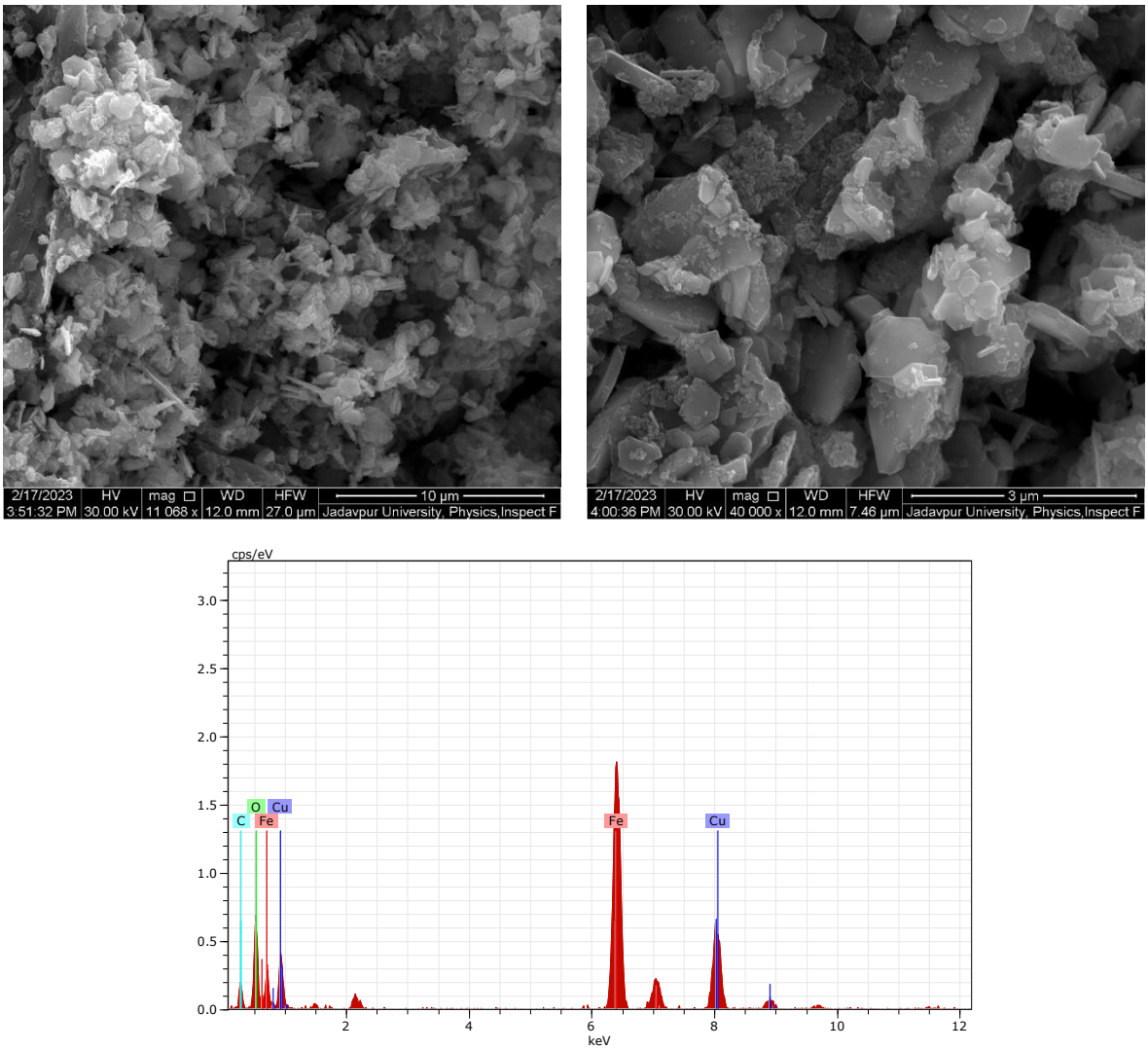

Figure 3: SEM Microscope and EDS Mapping of rGOCF

4.1.2 XRD Analysis:

The structural properties of GO, rGO, CF and rGOCF were investigated by X-ray diffraction (XRD). Fig. 4a shows the diffraction pattern of GO and it exhibits a peak at 2Θ = 10.6˚ with a corresponding d-spacing of 0.79 nm. In the XRD pattern of rGO (Fig. 4b) the peak was found at 2Θ = 23.2˚ with a corresponding d-spacing of 0.38 nm.

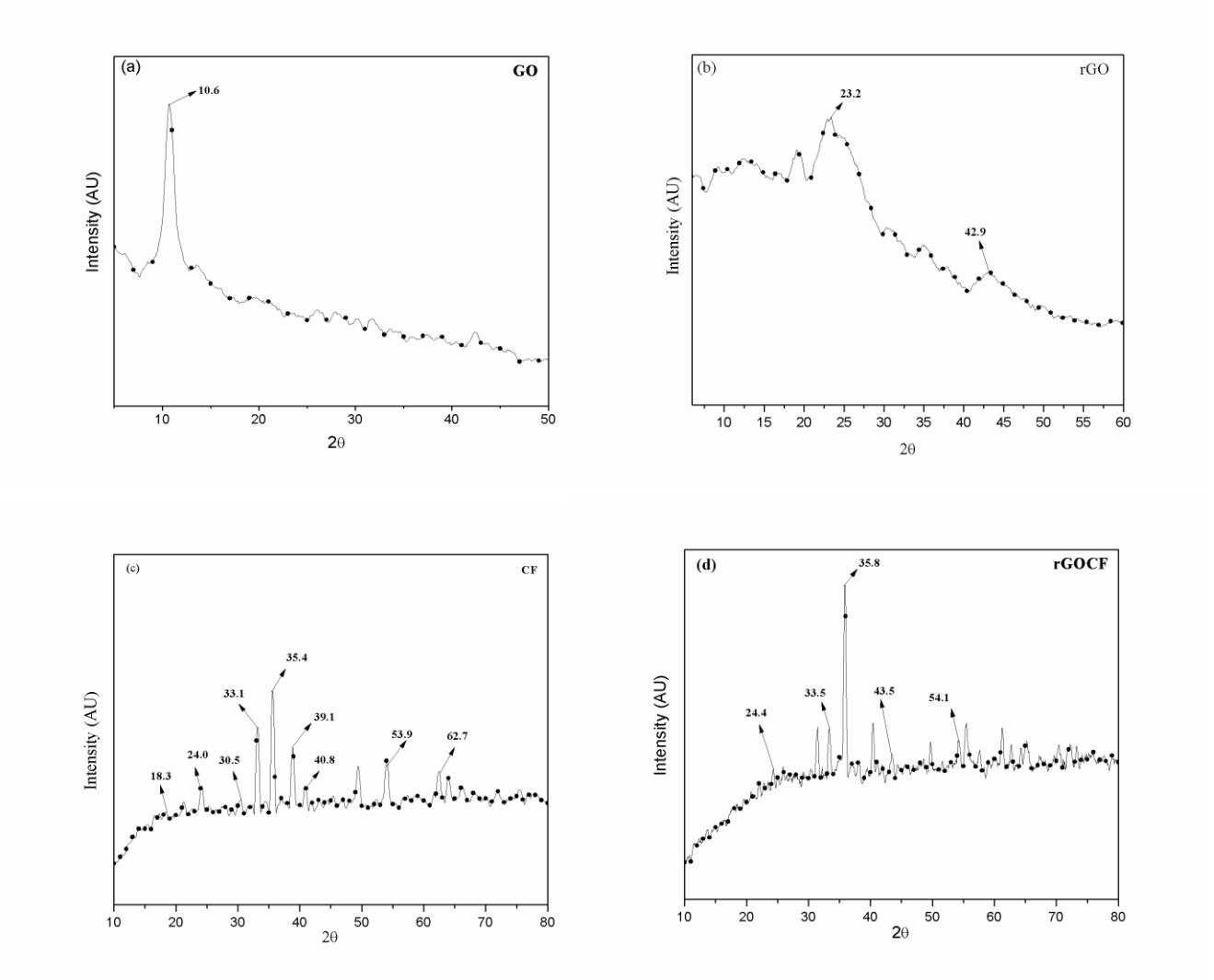

Figure 4: XRD Analysis of a. GO, b. rGO, c. CF, d. rGOCF

The decrease in the d-spacing value concludes the fact that the oxygenated functional groups initially present in the layers of GO were eliminated when GO was reduced to rGO and that is why the d-spacing value of rGO got decreased. The peak at 2Θ = 42.9˚ of rGO was due to the turbostratic band of disordered carbon material. The diffraction peaks of CF (Fig. 4c) confirms the presence of cubic and tetragonal phase of $CuFe_2O_4$ which exhibits high intensity with CuO and α-

Fe_2O_3 with low-intensity peak. The peak at 2Θ = 24˚ and 33.1˚ corresponds to the α-Fe_2O_3 whereas the appearance of the peak at 2Θ = 40.8˚ corresponds to the CuO. The peaks at 2Θ = 35.4˚ and 62.7˚ confirm the presence of cubic phase $CuFe_2O_4$ and the peaks at 2Θ = 18.3˚, 30.5˚ and 53.9˚ confirms the presence of tetragonal $CuFe_2O_4$ [55]–[57]. The results were in agreement with the JCPDS 25-0283 and JCPDS 34-0425. The diffraction peaks of rGOCF (Fig. 4d) was similar to CF which confirms the presence of cubic and tetragonal phase of CF. The diffraction peak of rGO in Fig. 4b was not visible due to the low intensity of rGO compared to CF. The average crystallite size was found by using the Debye-Scherrer formula.

Table 2: XRD Parameters

Sample	Average Crystallite Size (nm)	d-spacing (Å)
GO	44.49	7.90
rGO	15.22	3.83
CF	35.57	2.53
rGOCF	36.06	2.50

4.1.3 FTIR Analysis:

Fig.3 shows the FTIR spectra of GO, rGO, CF and rGOCF which were analysed in the wavenumber range of 4000 cm^{-1} to 500 cm^{-1}. In the FTIR spectra of GO (Fig. 5a) the broad peak at 3304 cm^{-1} was due to the stretching of hydroxyl group. The low-intensity peak at 1712 cm^{-1} was due to the carboxyl group. A sharp peak at 1585 cm^{-1} confirmed the presence of stretching and bending of the OH group. It happened due to the absorption of water by GO. The presence of the C-OH group was confirmed by 1356 cm^{-1}. The C-O-C stretching and vibrational mode of C-O were confirmed by the wavenumber of 1220 cm^{-1} and 1036 cm^{-1} respectively. Several oxygenated functional groups were present in the GO sample which were not available in the rGO FTIR spectra (Fig. 5b). The low-intensity peak at 3339 cm^{-1} was due to the stretching of the hydroxyl group. The peak at 1605 cm^{-1} in rGO shows a strong band, this suggests the recovery of the sp^2 lattice[58]–[60]. The peak at 3121 cm^{-1} of the FTIR spectra of CF (Fig. 5c) represents the -OH group. The peaks in the range between 1000 cm^{-1} to 500 cm^{-1} represent the metal-oxygen stretching vibration. The presence of the FeOOH system was confirmed by the peak at 930 cm^{-1}. The tetrahedral and octahedral phases of Fe-O bonds were present at 513 cm^{-1} and 805 cm^{-1}. The octahedral phase of

Cu-O was there at 426 cm^{-1} [61]. The peaks of FTIR spectra of rGOCF (Fig. 5d) were slightly shifted with compare to the FTIR spectra of rGO and CF due to the different chemical atmospheres.

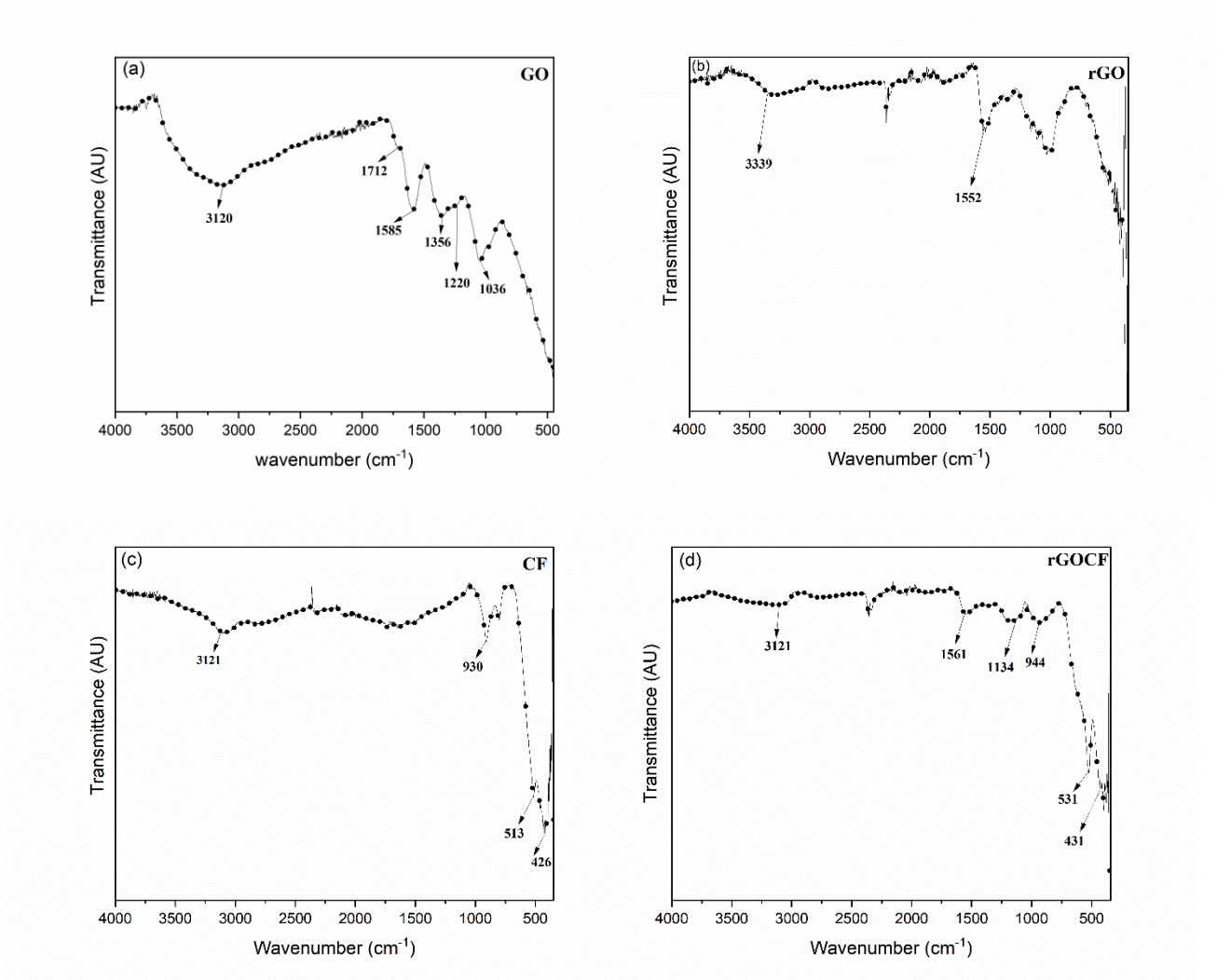

Figure 5: FTIR Spectrum of a. GO, b. rGO, c. CF, d. rGOCF

4.1.4 BET Study:

The BET method was used to calculate the surface area of rGOCF. The surface area was 20.92 $m^2.g^{-1}$ which was low due to the active sites of rGO being occupied by the CF composites. So fewer active sites were available for the nitrogen adsorption-desorption process. The adsorption-desorption curve (Fig. 6a) was following the type II isotherm with H_3 hysteresis. The average pore diameter was obtained from the BJH plot (Fig. 6b) which was approximately 3.3 nm. This confirms that the pores are mesopores which is also analogous with the H_3 type hysteresis. The average pore volume was 0.0417 $cm^3.g^{-1}$.

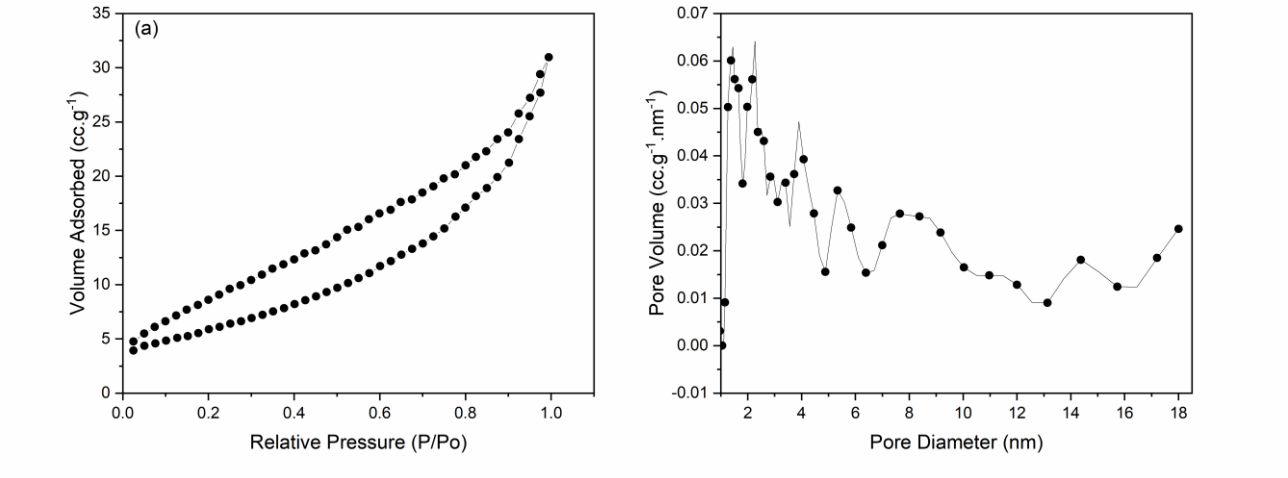

Figure 6: a. BET Adsorption Isotherm curve and b. BJH plot of rGOCF

4.1.5 UV-Vis Spectrophotoscopy Analysis:

A full-scale Ultra-Violet visible spectroscopy scan was done on the CF and rGOCF. The presence of copper ferrite is confirmed from the UV spectrum of CF (Fig. 7b) which shows the appearance of an absorbance band in the light region of 330-410 nm [62]. The peak due to CF is also visible

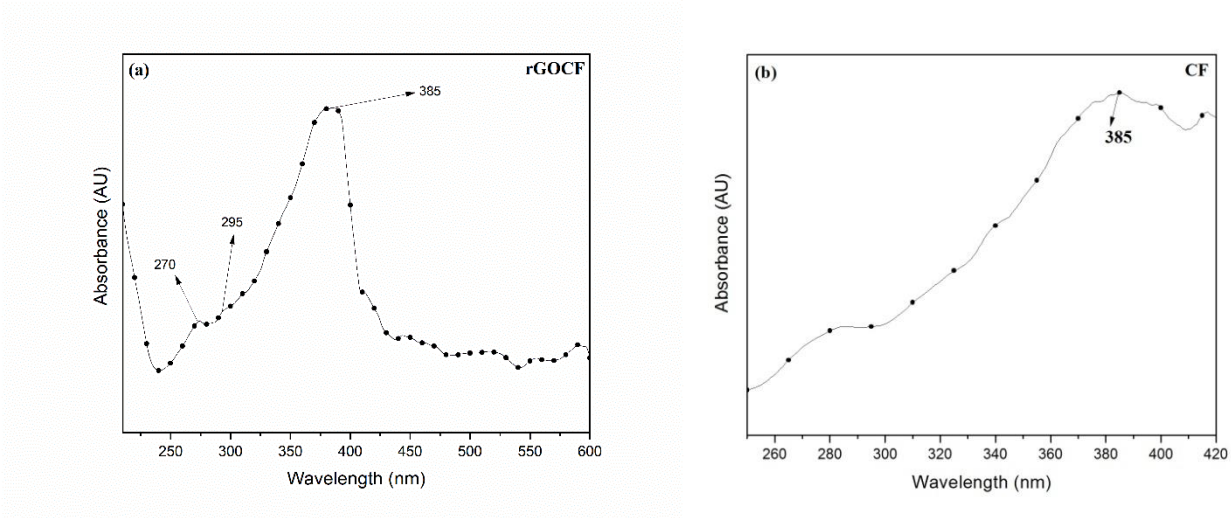

Figure 7: UV Spectrum of a. rGOCF and b.CF

in the range of 385 nm. The absorbance peak at 270 nm in the spectrum of rGOCF highlights the presence of rGO in fig. 7a.

4.2 EFFECT OF PARAMETERS

4.2.1 pH STUDY

The effect of pH was studied with an initial concentration of 90 ppm, adsorbent dosage of 50 mg/300 ml, Contact time was 2 hours and the pH was varied in the range of 1, 3, 5, 7, 9 and 11. The surface charge of rGOCF and NOR can be understood from this study. According to the result, at pH 7 the highest removal efficiency (~82%) was obtained. As we move away from the pH 7 to the acidic or basic side the removal efficiency decreased. This happens because the pH value of above 9.2 the surface charges of CF become negative and when the pH is below 6.5 the surface hydroxyl group is protonated to form OH_2^+ which generates positive charges over the surface[63]. On the other hand, the NOR have a piperazinyl and carboxyl functional group which exists in a different form in various pH. Its acid dissociation constants are 6.22 and 8.51. So, when the pH of the environment is greater than 8.5, NOR exists in anionic form and the pH is less than 6.2 the NOR exist in cationic form and the range between 6.2 and 8.5 NOR acts as a zwitter ion where the surface consists of an equal amount of positive and negative charge[64].

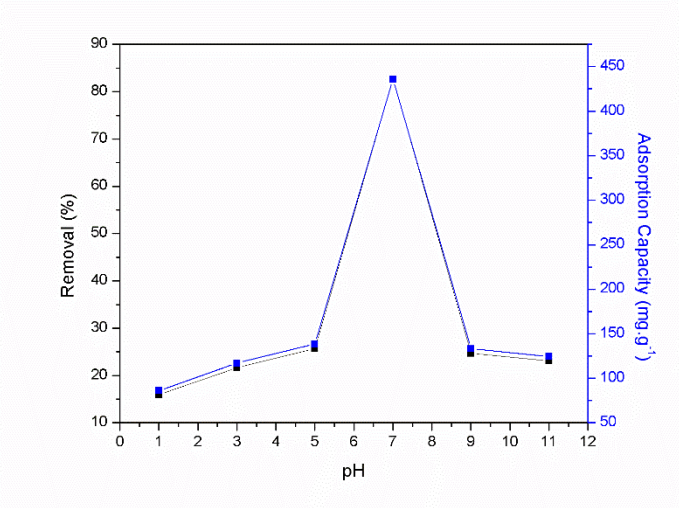

Figure 8: Effect of pH of NOR adsorption on rGOCF

4.2.2 Effect of Initial Concentration

This batch study was examined to understand the variation in removal efficiency and adsorption capacity. At pH 7 adsorbent dosage of 30 mg/300 ml, contact time of 2 hours and range of initial concentration – 15 ppm, 30 ppm, 45 ppm and 60 ppm were taken. As the initial concentration of NOR increased the removal efficiency decreased from 88.5% to 67.4%. But the adsorption capacity was gradually increased from 80 $mg.g^{-1}$ to 242 $mg.g^{-1}$. The adsorbent dosage was constant

so there were fixed numbers of active sites available. As the initial concentration of NOR increased the active sites were occupied early and as a result, the removal efficiency decreased. But in the case of adsorption capacity, fixed numbers of the active site of rGOCF were adsorbing increasing the initial concentration of NOR. Mathematically, the adsorbent dosage is inversely proportional to adsorption capacity. Fig. 9 shows the result of this study.

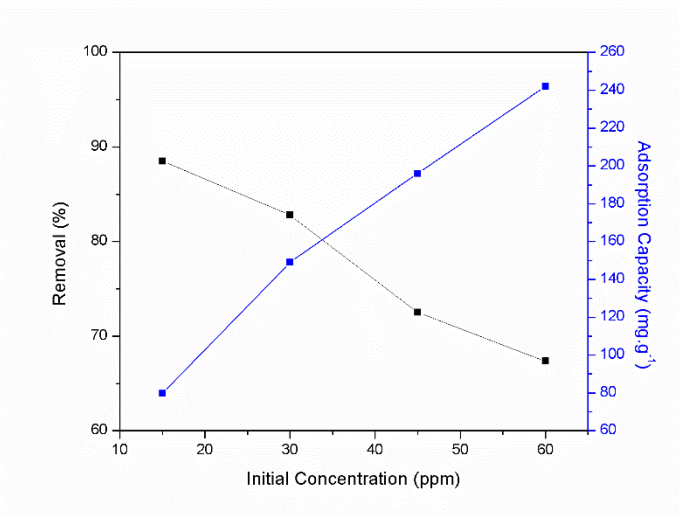

Figure 9: Effect Initial Concentration of NOR

4.2.3 Effect of Adsorbent Dosage

To find out the effect of adsorbent dosage, an initial concentration of NOR of 90 ppm, contact time of 2 hours and pH 7 were chosen as the batch study parameters.

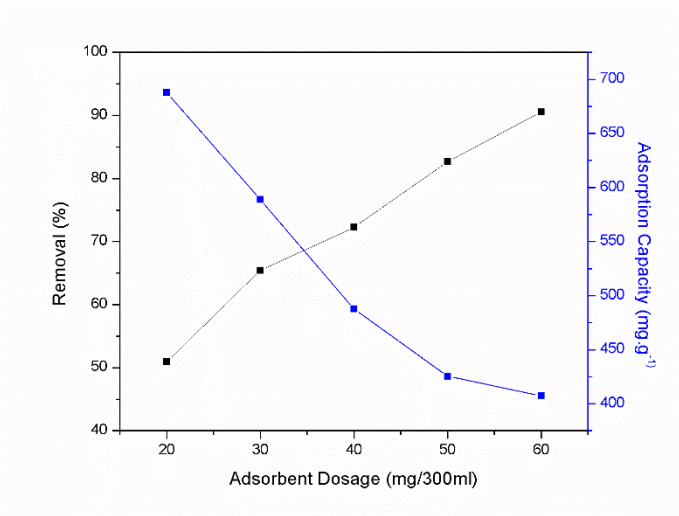

Figure 10: Effect of Adsorbent Dosage

The adsorbent dosage was varied like 20 mg, 30mg, 40 mg, 50 mg and 60mg. As a result (Fig. 8) the removal efficiency was increased from 50.94% to 90.55% whereas the adsorption capacity was decreased from 687.77 mg.g-1 to 407.47 mg.g-1. This happened because, at constant initial concentration, as the adsorbent dosage increased the active sites were also increased which enhance the removal efficiency. But high adsorbent dosage always decreases the adsorption capacity.

4.2.4 Effect of Contact Time

The contact time between adsorbent and adsorbate is required to find the time required to reach the equilibrium. At pH 7, an initial NOR concentration of 90 ppm and an adsorbent dosage of 50 mg/300 ml were chosen as the parameter. After the first 60 minutes, the removal efficiency was only about 75% with an adsorption capacity of 386 $mg.g^{-1}$. But at the end of 2 hours, the removal efficiency was 83% with an adsorption capacity of 415 $mg.g^{-1}$. Initially, the active sites of rGOCF were empty but as the time increased the active sites were getting occupied and after 2 hours the batch system reached equilibrium. Fig. 11 shows the result.

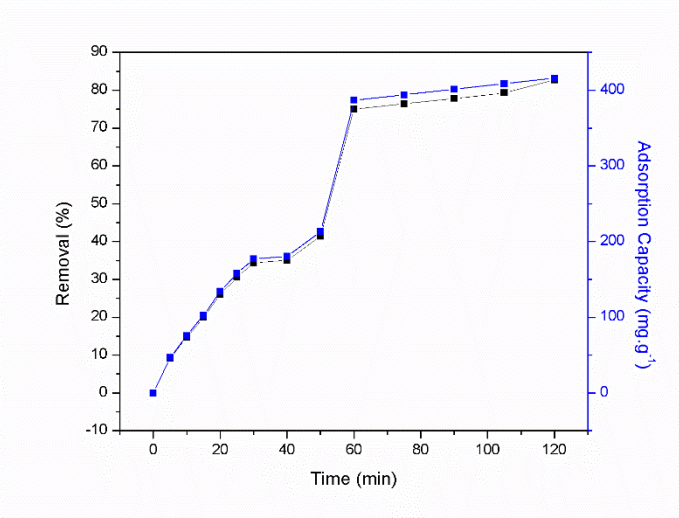

Figure11: Effect of Contact Time of NOR Adsorption on rGOCF

4.2.5 Effect of Temperature

The effect of temperature on the adsorption of NOR was studied in the temperature range of 303K to 333K. The initial concentration was 90 ppm, the adsorbent dosage was 50 mg and the contact time was 2 hours. As the temperature increased the removal efficiency also increased from 82% to

about 84.5%. This happened due to the expansion of pores which enhances the diffusion of NOR onto rGOCF.

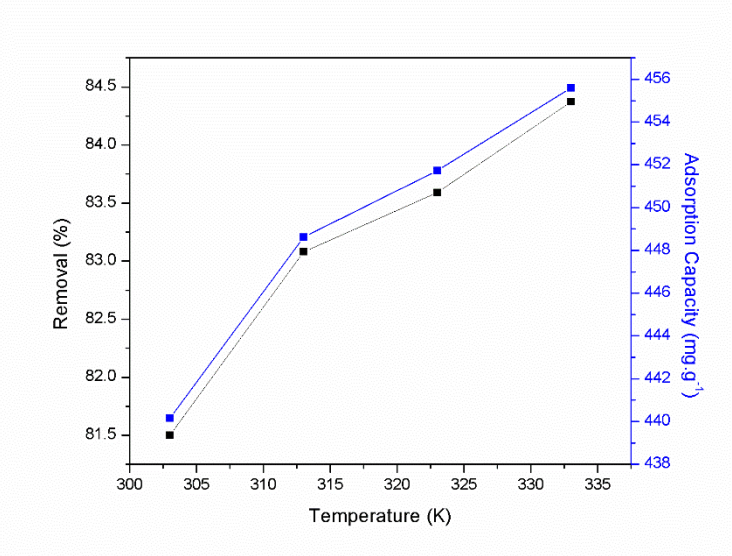

Figure 12: Effect of Temperature of NOR Adsorption on rGOCF

4.3 ADSORPTION ISOTHERM

The adsorption isotherms play a pivotal role to determine the adsorption performance.

Langmuir Isotherm: This is the first proposed isotherm for the gas adsorption on the solid with the assumptions like adsorption is occurring in a single layer, there are a fixed number of adsorptive sites, no steric hindrances between adsorbed molecules and adsorbent surface, no phase change. The mathematical expression is as follows,

$$Q_e = \frac{Q_{max} K_l C_e}{1 + K_l C_e}$$

Here, Q_e is the equilibrium adsorption capacity ($mg.g^{-1}$), K_L is the Langmuir Isotherm Constant ($L.mg^{-1}$) and C_e is the equilibrium adsorbate concentration ($mg.L^{-1}$). The linearized form of the above equation is,

$$\frac{C_e}{Q_e} = \frac{C_e}{Q_{max}} + \frac{1}{Q_{max} K_l}$$

There is another important factor present in this isotherm which is Separation Factor R_l. The expression is as follows,

$$R_l = \frac{1}{1 + K_l C_0}$$

Where C_0 is the maximum initial concentration ($mg.L^{-1}$). R_l value between 0 and 1 is favourable. The adsorption process is linear, unfavourable and irreversible for the following conditions $R_l = 1$, $R_l > 1$ and $R_l = 0$ respectively.

Freundlich Isotherm: This does not restrict monolayer adsorption and considers multilayer adsorption. The mathematical expression is as follows,

$$Q_e = K_f C_e^{1/n}$$

Here K_f and n are isotherm constants which describe the adsorption capacity and adsorption intensity respectively. Quantitative measurement of the adsorption intensity is provided by the value of 1/n between 0 and 1, which shifts to a less uniform distribution as the value approaches zero. On the other hand, a value of larger than 1 indicates cooperative adsorption, while a value of less than 1 indicates that a conventional Langmuir isotherm may explain the adsorption process without losing generality[65]. The linearized form of the isotherm equation is,

$$\log Q_e = \log K_f + \frac{1}{n} \log C_e$$

Temkin Isotherm: Following is the Temkin isotherm linear fit equation,

$$Q_e = B_T \ln K_T + B_T \ln C_e$$

Here B_T is the coefficient of heat of adsorption (J/mol) and K_T is the coefficient of adsorption capacity(L/mg). T is the experimental temperature (K).

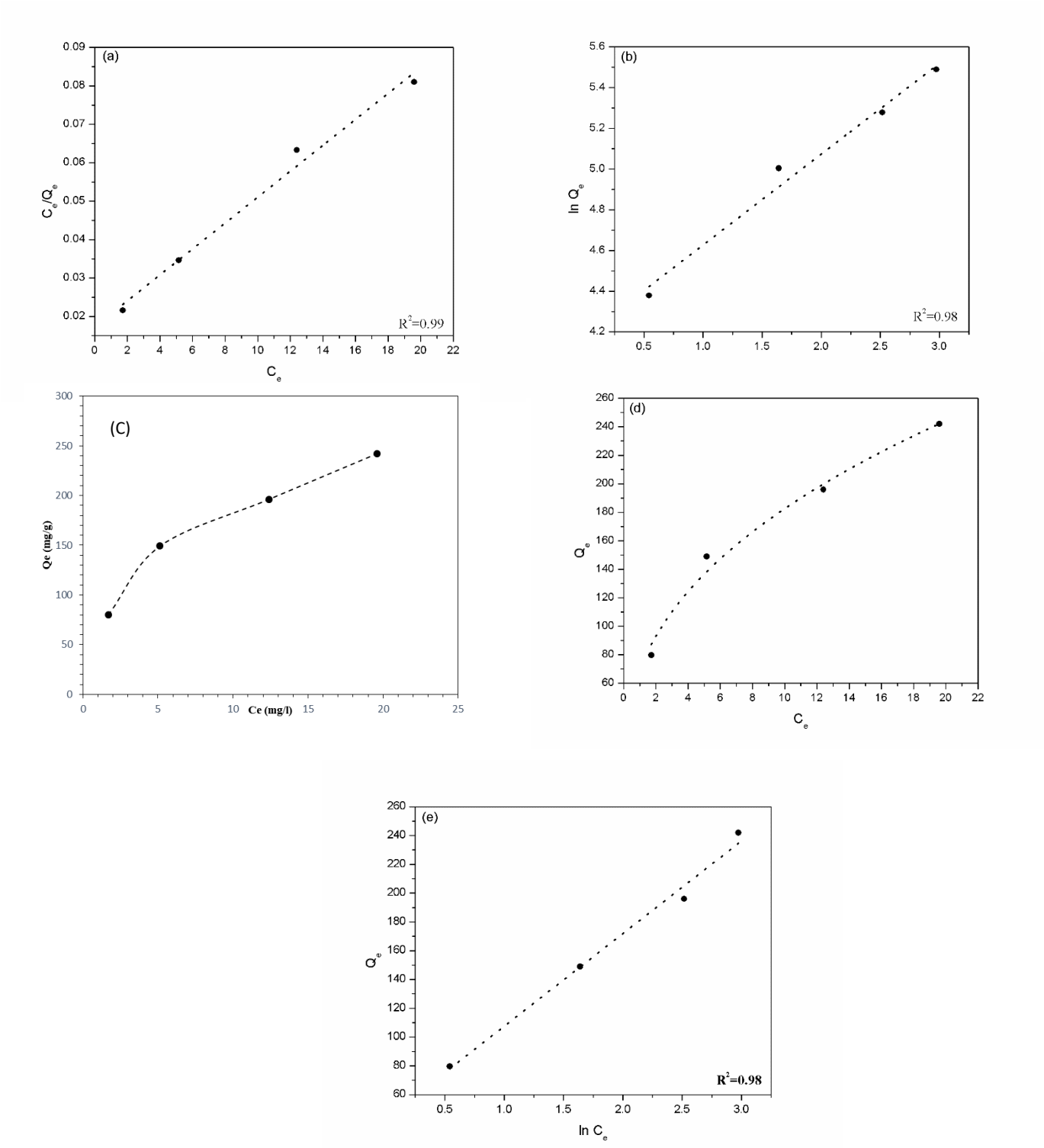

Figure13: a. Langmuir Isotherm Linear Fit, b. Freundlich Isotherm Linear Fit, c. Langmuir Isotherm Nonlinear Fit, d. Freundlich Isotherm Nonlinear Fit, e. Temkin Isotherm Linear Fit of nOR adsorption on rGOCF

The linear isotherm of Langmuir, Freundlich and Temkin isotherm and nonlinear Langmuir and Freundlich were analysed. From the R^2 value and RMS error value, it can be concluded that Langmuir linear isotherm fitted best for this study. For nonlinear isotherms also, Langmuir isotherm is the best option to explain the process. So, the adsorption following Langmuir isotherm suggests that the adsorption happens in the monolayer mechanism.

Table 3: Linear Adsorption Isotherm Parameters

Model	Parameter	Values
Langmuir	K_l	0.19
	R_l	0.0806
	Q_{max}	296.74
	R^2	0.9934
	RMSE error	0.000025
Freundlich	K_F	65.442
	1/n	0.4461
	R^2	0.9838
	RMSE error	0.01131
Temkin	K_T	1.957
	B_T	64.33858
	R^2	0.98

Table 4: Nonlinear Adsorption Isotherm

Model	Parameters	Values
Langmuir	K_l	0.2
	R_l	0.0769
	Q_{max}	292.11
	X^2	1.410
Freundlich	K_F	69.5
	1/n	0.42

	Chi-Square	92.74

4.4 ADSORPTION KINETICS

Understanding the adsorption rate, mechanism, and effectiveness requires knowledge of adsorption kinetics. The design of an adsorption system must take into account the adsorption kinetics. pseudo-first-order, pseudo-second-order and Intra particle diffusion kinetics had studied in this experiment.

Pseudo-first-order Kinetics: It assumes one of the reactants is at an abundant amount and so the change in the concentration is negligible. The linear form of this equation is given below,

$$\ln(Q_e - Q_t) = -K_1.t + \ln Q_e$$

Here, Q_e and Q_t are the adsorption capacity at equilibrium and at any time t respectively and K_1 is the kinetics constant

Pseudo-second-order Kinetics: The linearized form of kinetics equation is,

$$\frac{t}{Q_t} = \frac{t}{Q_e} + \frac{1}{K_2 Q_e^2}$$

Intra-particle Diffusion: The diffusion of adsorbate molecules can be studied by the intra-particle diffusion model.

$$Q_e = K_p t^{0.5}$$

K_p is the inter-particle diffusion rate constant ($mg.g^{-1}.min^{-0.5}$) which can be found from the Q_e vs $t^{0.5}$ plot.

Pseudo-second-order kinetics is dominant as it has a larger R^2 value and lesser error. So it can be stated that the process is following pseudo-second-order kinetics. Following a pseudo-second-order reaction means there is more chance of the reaction following the chemisorption process as compared to physisorption.

The π-electron acceptor and electron donor interaction are developed because of the F-atom present on the benzene ring of NOR which shows an electron-withdrawing effect that makes the aromatic ring π-electron acceptor. The OH^- group present in the adsorbent act as the electron donor.

The π-electron acceptor of NOR and electron donor of adsorbent stimulate the adsorption process[66].

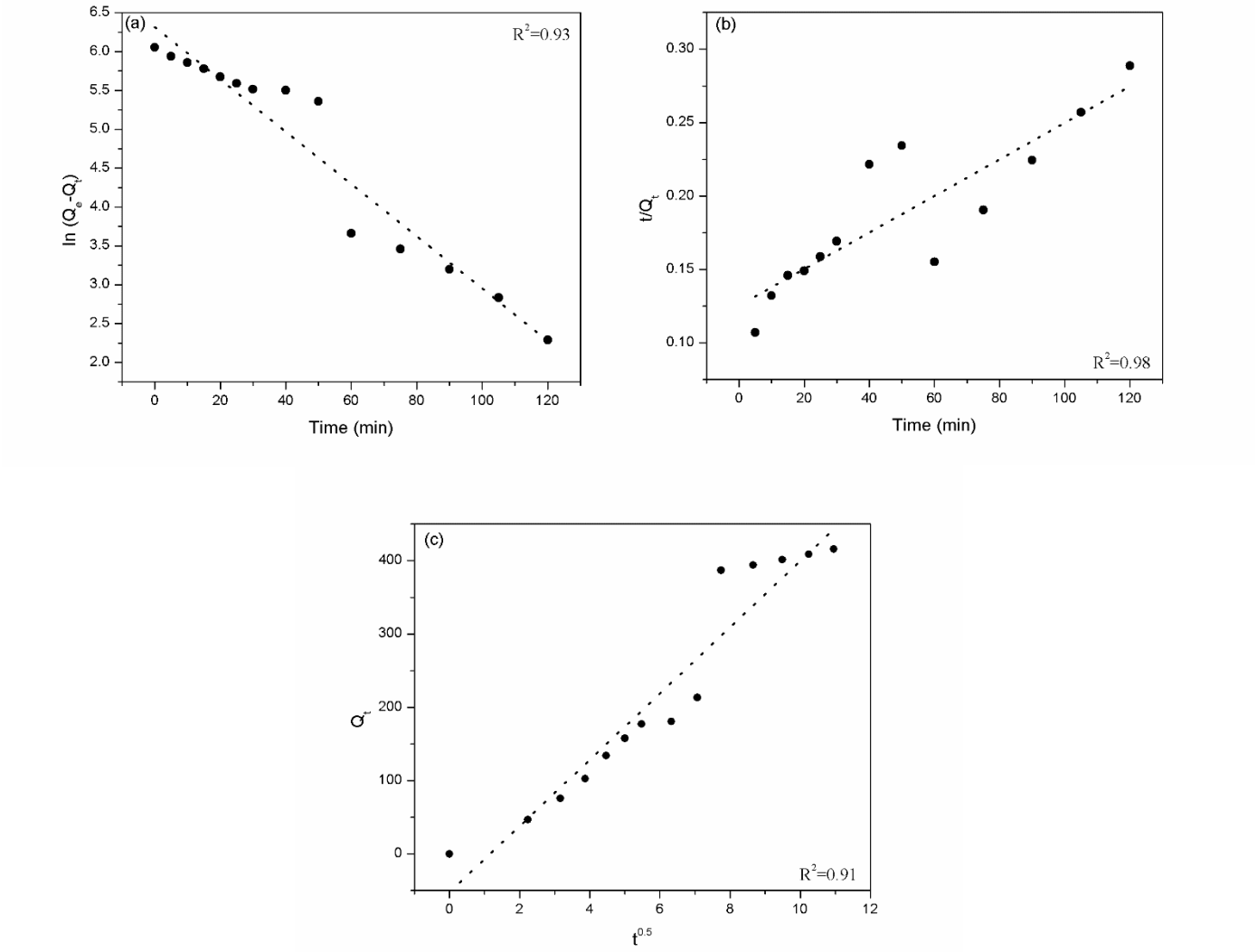

Figure 14: a. Pseudo-first-order Kinetics, b. Pseudo-second-order Kinetics, c. Intra-particle Diffusion of NOR Adsorption on rGOCF

Table 5: Adsorption Kinetics Data

Models	Parameters	Values
Pseudo-first order	K_1	0.03363
	Q_e	552.27
	R^2	0.93523

	RMSE error	0.2973391
Pseudo-second order	K_2	0.00001225
	Q_e	806.45
	R^2	0.98254
	RMSE error	0.01077356
Intra-particle Diffusion	K_P	45
	R^2	0.91

4.5 ADSORPTION THERMODYNAMICS

Batch adsorption processes were carried out at different temperatures – 30^0C, 40^0C, 50^0C and 60^0C to understand the thermodynamics of the adsorption process. The results obtained from these experiments were used to find out thermodynamic parameters like Gibbs free energy change ($\Delta G_{adsorption}$), change of enthalpy ($\Delta H_{adsorption}$), change in entropy ($\Delta S_{adsorption}$) and equilibrium constant (K_C). Following are the equations used in this study,

$$\ln K_c = \frac{\Delta S}{R} - \frac{\Delta H}{RT}$$

$$\Delta G = \Delta H - T\Delta S$$

$$Kc = \frac{Q_e}{C_e}$$

Here, Q_e and C_e are the equilibrium adsorption capacity and equilibrium concentration of the adsorbate. R is the universal gas constant 8.314 $J.mol^{-1}.K^{-1}$

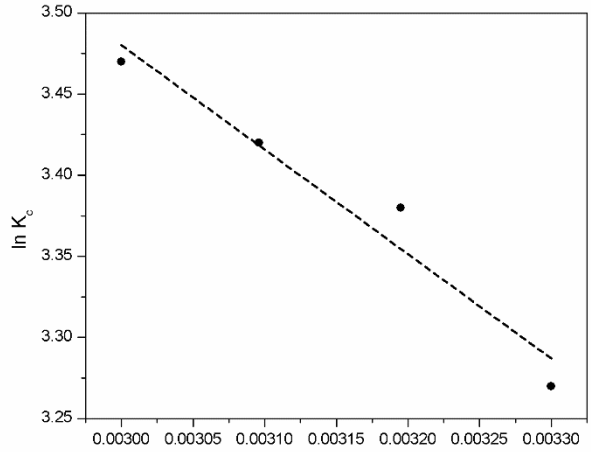

Figure 15: Thermodynamics Study of NOR adsorption on rGOCF

Table 6: Adsorption Thermodynamics Data

Temperature (K)	C_e(ppm)	Q_e(mg/g)	K_C	$\Delta G_{adsorption}$(J/mol)	$\Delta H_{adsorption}$(J/mol)	$\Delta S_{adsorption}$ (J/mol.K)
303	16.64	440.16	26.45	-8277.57		
313	15.23	448.62	29.46	-8727.22	5348.39	44.97
323	14.77	451.74	30.58	-9176.92		
333	14.07	455.58	32.37	-9626.62		

The $\Delta H_{adsorption}$ shows a positive value as the temperature increases. This is because when the temperature increases the internal energy of the system increases. Now enthalpy change is directly proportional to internal energy change. That is why, $\Delta H_{adsorption}$shows a positive value. As the temperature increases, the kinetic energy of the system also increases. Higher kinetic energy means higher randomness of the molecules in the system. So, the $\Delta S_{adsorption}$showed a positive value. Negative Gibbs free energy change indicates that the process is spontaneous. The process is more spontaneous as the temperature increases.

4.6 REGENERATION STUDY

A regeneration study (Fig. 14) was done to find out how economical the adsorbent is. After each cycle, the adsorbent was washed with a 10:1 ratio solution of ethanol and HCl. Then the adsorbent was washed with water by vacuum filtration to neutralize the pH. Then the adsorbent was dried in a hot air oven at 60^0C for 24 hours. The initial NOR concentration was taken as 200 ppm. The adsorbent dosage was 100 mg. The removal efficiency decreased from 86.2% to 72.5% after 5 cycles of batch adsorption. Though the removal efficiency decreased, after 5 cycles, it was pretty high. So it can be concluded that the ethanol/HCl (10:1) solution is pretty effective to dissolve NOR and wash out the adsorbent rGOCF.

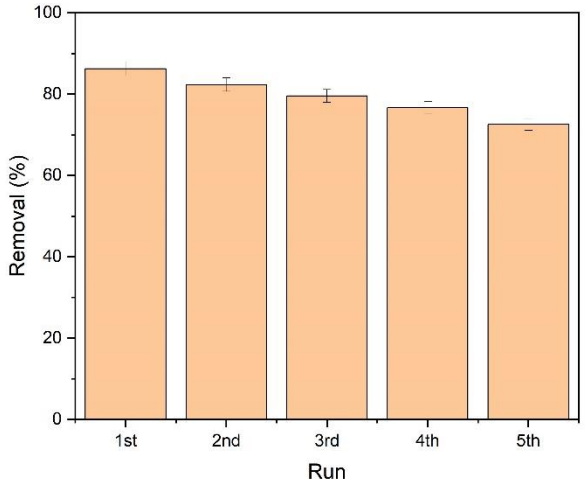

Figure 16: Regeneration Study of NOR Adsorption on rGOCF

CHAPTER 5: CONCLUSION

5.1 CONCLUSION

Graphene Oxide has been synthesized from graphite flakes by modified Hummer's Method. Then the graphene oxide is reduced by 6 (M) NaOH solution. Then by hydrothermal process and with the help of hydrated copper and iron salt reduced graphene oxide-based copper ferrite composite adsorbent is prepared. The SEM, XRD, FTIR and BET analysis was done to characterize the adsorbent. The SEM result shows the successful deposition of copper ferrite on the reduced graphene oxide flakes. The EDS result shows the weight percentage of each element and also ensures that there are no impurities in the adsorbent. With the help of XRD data, the maximum reduction of graphene oxide into reduced graphene oxide has been observed. The formation of $CuFe_2O_4$ and a small amount of CuO has been confirmed by the XRD analysis of copper ferrite. The FTIR result shows that the number of oxygen-containing functional groups present in the graphene oxide decreases when graphene oxide reduces into reduced graphene oxide. The BET analysis gives a surface area of 20.92 $m^2.g^{-1}$ and a pore volume of 0.0417 $cc.g^{-1}$. pH study shows that at pH 7 the maximum removal efficiency has been attained. The effect of initial adsorbate concentration shows that as we increase the initial concentration of the NOR for a fixed amount of adsorbent, the removal efficiency decreases. On the other hand in the case of adsorbent dosage if we increase the adsorbent dosage for a fixed amount of initial NOR concentration the removal efficiency increases. The opposite results happen because in the case of initial NOR concentration, the number of active sites in the adsorbent is fixed but the number of molecules of NOR is increasing. So the active sites are getting occupied and the rest of the NOR molecules become unadsorbed. So the adsorptive removal efficiency keeps decreasing. But in the case of adsorbent dosage, the number of active sites increased but the number of NOR molecules is fixed. So, there are more free active sites available for adsorption which promote the adsorption. In the study of contact time, the rate of adsorption was quite high at the beginning of the process. But as time moves forward, the active sites were getting occupied so the rate of adsorption was decreasing. After 2 hours the process reached the equilibrium stage. A Kinetics study was done on pseudo-first-order kinetics and pseudo-second-order kinetics. Pseudo-second-order kinetics shows a bigger R^2 value and smaller error compared to pseudo-first-order kinetics. So, it can be concluded the process has followed pseudo-second-order kinetics. In the isotherm analysis, Langmuir and Freundlich's isotherm studied. Both linear and nonlinear fit were examined. The Langmuir isotherm shows better results in both linear and nonlinear fit with a maximum adsorption capacity

of 296.74 $mg.g^{-1}$. The regeneration study was done up to 5 batch adsorption cycles. The removal efficiency dropped from 86.2 % to 72.5%. So, the ethanol/HCl (10:1) solution is capable of washing the adsorbent of NOR adsorption.

REFERENCES:

[1] M. S. Fram and K. Belitz, "Occurrence and concentrations of pharmaceutical compounds in groundwater used for public drinking-water supply in California," *Science of The Total Environment*, vol. 409, no. 18, pp. 3409–3417, Aug. 2011, doi: 10.1016/J.SCITOTENV.2011.05.053.

[2] A. Küster and N. Adler, "Pharmaceuticals in the environment: scientific evidence of risks and its regulation.," *Philos Trans R Soc Lond B Biol Sci*, vol. 369, no. 1656, Nov. 2014, doi: 10.1098/rstb.2013.0587.

[3] G. Yang, M. Fan, and G. Zhang, "Emerging contaminants in surface waters in China - A short review," *Environmental Research Letters*, vol. 9, no. 7. Institute of Physics Publishing, Jul. 01, 2014. doi: 10.1088/1748-9326/9/7/074018.

[4] C. Munthe, N. Nijsingh, K. de F. Licht, and D. G. J. Larsson, "Health-related research ethics and social value: Antibiotic resistance intervention research and pragmatic risks," *Transplant International*, vol. 32, no. 4, pp. 209–224, Apr. 2019, doi: 10.1111/bioe.12580.

[5] T. P. Van Boeckel *et al.*, "Global trends in antimicrobial use in food animals," *Proceedings of the National Academy of Sciences*, vol. 112, no. 18, pp. 5649–5654, May 2015, doi: 10.1073/pnas.1503141112.

[6] B. Kinsella *et al.*, "Current trends in sample preparation for growth promoter and veterinary drug residue analysis.," *J Chromatogr A*, vol. 1216, no. 46, pp. 7977–8015, Nov. 2009, doi: 10.1016/j.chroma.2009.09.005.

[7] F. Wang *et al.*, "Effects of antibiotic norfloxacin on the degradation and enantioselectivity of the herbicides in aquatic environment," *Ecotoxicol Environ Saf*, vol. 208, Jan. 2021, doi: 10.1016/j.ecoenv.2020.111717.

[8] M. Wang, W. Shen, L. Yan, X. H. Wang, and H. Xu, "Stepwise impact of urban wastewater treatment on the bacterial community structure, antibiotic contents, and prevalence of antimicrobial resistance," *Environmental Pollution*, vol. 231, pp. 1578–1585, Dec. 2017, doi: 10.1016/j.envpol.2017.09.055.

[9] Y. Guo, P. S. Qi, and Y. Z. Liu, “A Review on Advanced Treatment of Pharmaceutical Wastewater,” in *IOP Conference Series: Earth and Environmental Science*, Institute of Physics Publishing, May 2017. doi: 10.1088/1755-1315/63/1/012025.

[10] A. S. Eltaweil *et al.*, “Chitosan based adsorbents for the removal of phosphate and nitrate: A critical review,” *Carbohydr Polym*, vol. 274, p. 118671, Nov. 2021, doi: 10.1016/j.carbpol.2021.118671.

[11] G. Perot and M. Guisnet, “Advantages and disadvantages of zeolites as catalysts in organic chemistry,” *Journal of Molecular Catalysis*, vol. 61, no. 2, pp. 173–196, Aug. 1990, doi: 10.1016/0304-5102(90)85154-A.

[12] M. Tawalbeh, A. Al-Othman, N. Ashoobi, and M. Alkasrawi, “Classifications of Thermal Energy Storage Materials,” in *Encyclopedia of Smart Materials*, Elsevier, 2022, pp. 450–469. doi: 10.1016/B978-0-12-815732-9.00064-4.

[13] L. P. Lingamdinne, Y. L. Choi, I. S. Kim, J. K. Yang, J. R. Koduru, and Y. Y. Chang, “Preparation and characterization of porous reduced graphene oxide based inverse spinel nickel ferrite nanocomposite for adsorption removal of radionuclides,” *J Hazard Mater*, vol. 326, pp. 145–156, 2017, doi: 10.1016/j.jhazmat.2016.12.035.

[14] L. Zhang, Y. Tian, Y. Guo, H. Gao, H. Li, and S. Yan, “Introduction of α-MnO2 nanosheets to NH2 graphene to remove Cr6+ from aqueous solutions,” *RSC Adv*, vol. 5, no. 55, pp. 44096–44106, 2015, doi: 10.1039/c5ra04545b.

[15] W. Zhang, X. Shi, Y. Zhang, W. Gu, B. Li, and Y. Xian, “Synthesis of water-soluble magnetic graphene nanocomposites for recyclable removal of heavy metal ions,” *J Mater Chem A Mater*, vol. 1, no. 5, pp. 1745–1753, Feb. 2013, doi: 10.1039/c2ta00294a.

[16] K. Zaharieva *et al.*, “Preparation, characterization and application of nanosized copper ferrite photocatalysts for dye degradation under UV irradiation,” *Mater Chem Phys*, vol. 160, pp. 271–278, Jun. 2015, doi: 10.1016/j.matchemphys.2015.04.036.

[17] M. M. Rashad, R. M. Mohamed, M. A. Ibrahim, L. F. M. Ismail, and E. A. Abdel-Aal, “Magnetic and catalytic properties of cubic copper ferrite nanopowders synthesized from

secondary resources," *Advanced Powder Technology*, vol. 23, no. 3, pp. 315–323, May 2012, doi: 10.1016/j.apt.2011.04.005.

[18] J. Calvo-De La Rosa and M. Segarra, "Optimization of the Synthesis of Copper Ferrite Nanoparticles by a Polymer-Assisted Sol-Gel Method," *ACS Omega*, vol. 4, no. 19, pp. 18289–18298, Nov. 2019, doi: 10.1021/acsomega.9b02295.

[19] I. Nedkov, R. E. Vandenberghe, T. Marinova, P. Thailhades, T. Merodiiska, and I. Avramova, "Magnetic structure and collective Jahn-Teller distortions in nanostructured particles of CuFe 2 O 4," *Appl Surf Sci*, vol. 253, no. 5, pp. 2589–2596, Dec. 2006, doi: 10.1016/j.apsusc.2006.05.049.

[20] S. Mishra, R. Acharya, and K. Parida, "Spinel-Ferrite-Decorated Graphene-Based Nanocomposites for Enhanced Photocatalytic Detoxification of Organic Dyes in Aqueous Medium: A Review," *Water (Switzerland)*, vol. 15, no. 1. MDPI, Jan. 01, 2023. doi: 10.3390/w15010081.

[21] Z. Iqbal, M. S. Tanweer, and M. Alam, "Reduced Graphene Oxide-Modified Spinel Cobalt Ferrite Nanocomposite: Synthesis, Characterization, and Its Superior Adsorption Performance for Dyes and Heavy Metals," *ACS Omega*, vol. 8, no. 7, pp. 6376–6390, Feb. 2023, doi: 10.1021/acsomega.2c06636.

[22] A. Al Nafiey *et al.*, "Reduced graphene oxide decorated with Co3O4 nanoparticles (rGO-Co3O4) nanocomposite: A reusable catalyst for highly efficient reduction of 4-nitrophenol, and Cr(VI) and dye removal from aqueous solutions."

[23] A. R. B. Bayantong, Y. J. Shih, D. C. Ong, R. R. M. Abarca, C. Di Dong, and M. D. G. de Luna, "Adsorptive removal of dye in wastewater by metal ferrite-enabled graphene oxide nanocomposites," *Chemosphere*, vol. 274, Jul. 2021, doi: 10.1016/j.chemosphere.2020.129518.

[24] N. Kaur, M. Kaur, and D. Singh, "Fabrication of mesoporous nanocomposite of graphene oxide with magnesium ferrite for efficient sequestration of Ni (II) and Pb (II) ions: Adsorption, thermodynamic and kinetic studies," *Environmental Pollution*, vol. 253, pp. 111–119, Oct. 2019, doi: 10.1016/j.envpol.2019.05.145.

[25] Y.-J. Tu, C.-F. You, C.-K. Chang, T.-S. Chan, and S.-H. Li, "XANES evidence of molybdenum adsorption onto novel fabricated nano-magnetic CuFe2O4," *Chemical Engineering Journal*, vol. 244, pp. 343–349, May 2014, doi: 10.1016/j.cej.2014.01.084.

[26] Y. Ren *et al.*, "Adsorption of Pb(II) and Cu(II) from aqueous solution on magnetic porous ferrospinel MnFe 2O 4," *J Colloid Interface Sci*, vol. 367, no. 1, pp. 415–421, Feb. 2012, doi: 10.1016/j.jcis.2011.10.022.

[27] Z. Li, Y. Ma, and L. Qi, "Formation of nickel-doped magnetite hollow nanospheres with high specific surface area and superior removal capability for organic molecules," *Nanotechnology*, vol. 27, no. 48, p. 485601, Dec. 2016, doi: 10.1088/0957-4484/27/48/485601.

[28] A.-S. A. Bakr, Y. M. Moustafa, E. A. Motawea, M. M. Yehia, and M. M. H. Khalil, "Removal of ferrous ions from their aqueous solutions onto NiFe2O4–alginate composite beads," *J Environ Chem Eng*, vol. 3, no. 3, pp. 1486–1496, Sep. 2015, doi: 10.1016/j.jece.2015.05.020.

[29] S. Zhang, H. Niu, Y. Cai, X. Zhao, and Y. Shi, "Arsenite and arsenate adsorption on coprecipitated bimetal oxide magnetic nanomaterials: MnFe2O4 and CoFe2O4," *Chemical Engineering Journal*, vol. 158, no. 3, pp. 599–607, Apr. 2010, doi: 10.1016/j.cej.2010.02.013.

[30] B. Bateer *et al.*, "Synthesis, size and magnetic properties of controllable MnFe 2O4 nanoparticles with versatile surface functionalities," *Dalton Transactions*, vol. 43, no. 26, pp. 9885–9891, Jul. 2014, doi: 10.1039/c4dt00089g.

[31] Y. J. Tu, C. F. You, and C. K. Chang, "Kinetics and thermodynamics of adsorption for Cd on green manufactured nano-particles," *J Hazard Mater*, vol. 235–236, pp. 116–122, Oct. 2012, doi: 10.1016/j.jhazmat.2012.07.030.

[32] W. Sun, W. Pan, F. Wang, and N. Xu, "Removal of Se(IV) and Se(VI) by MFe2O4 nanoparticles from aqueous solution," *Chemical Engineering Journal*, vol. 273, pp. 353–362, Aug. 2015, doi: 10.1016/j.cej.2015.03.061.

[33] S. Zeng, S. Duan, R. Tang, L. Li, C. Liu, and D. Sun, "Magnetically separable Ni0.6Fe2.4O4 nanoparticles as an effective adsorbent for dye removal: Synthesis and study on the kinetic and thermodynamic behaviors for dye adsorption," *Chemical Engineering Journal*, vol. 258, pp. 218–228, Dec. 2014, doi: 10.1016/j.cej.2014.07.093.

[34] L. Yang *et al.*, "The investigation of synergistic and competitive interaction between dye Congo red and methyl blue on magnetic MnFe2O4," *Chemical Engineering Journal*, vol. 246, pp. 88–96, Jun. 2014, doi: 10.1016/j.cej.2014.02.044.

[35] J. Feng *et al.*, "Synthesis of magnetic ZnO/ZnFe2O4 by a microwave combustion method, and its high rate of adsorption of methylene blue," *J Colloid Interface Sci*, vol. 438, pp. 318–322, Jan. 2015, doi: 10.1016/j.jcis.2014.10.009.

[36] R. Wu, J. Qu, H. He, and Y. Yu, "Removal of azo-dye Acid Red B (ARB) by adsorption and catalytic combustion using magnetic CuFe2O4 powder," *Appl Catal B*, vol. 48, no. 1, pp. 49–56, Mar. 2004, doi: 10.1016/j.apcatb.2003.09.006.

[37] M. A. Rehman, I. Yusoff, and Y. Alias, "Fluoride adsorption by doped and un-doped magnetic ferrites CuCexFe2-xO4: Preparation, characterization, optimization and modeling for effectual remediation technologies," *J Hazard Mater*, vol. 299, pp. 316–324, Dec. 2015, doi: 10.1016/j.jhazmat.2015.06.030.

[38] Y. J. Tu and C. F. You, "Phosphorus adsorption onto green synthesized nano-bimetal ferrites: Equilibrium, kinetic and thermodynamic investigation," *Chemical Engineering Journal*, vol. 251, pp. 285–292, Sep. 2014, doi: 10.1016/j.cej.2014.04.036.

[39] E. Al-Hetlani, B. D'Cruz, M. O. Amin, and M. Madkour, "An effective magnetic nanoadsorbent based on a carbonaceous/spinel ferrite nanocomposite for the removal of pharmaceutical pollutants from wastewater," *Environ Sci (Camb)*, vol. 8, no. 5, pp. 998–1010, 2022, doi: 10.1039/D1EW00495F.

[40] Z. Jia, Q. Wang, J. Liu, L. Xu, and R. Zhu, "Effective removal of phosphate from aqueous solution using mesoporous rodlike NiFe2O4 as magnetically separable adsorbent," *Colloids Surf A Physicochem Eng Asp*, vol. 436, pp. 495–503, 2013, doi: 10.1016/j.colsurfa.2013.07.025.

[41] F. A. Jumeri *et al.*, "Microwave synthesis of magnetically separable ZnFe2O 4-reduced graphene oxide for wastewater treatment," *Ceram Int*, vol. 40, no. 5, pp. 7057–7065, Jun. 2014, doi: 10.1016/j.ceramint.2013.12.037.

[42] E. K. Putra, R. Pranowo, J. Sunarso, N. Indraswati, and S. Ismadji, "Performance of activated carbon and bentonite for adsorption of amoxicillin from wastewater: Mechanisms, isotherms and kinetics," *Water Res*, vol. 43, no. 9, pp. 2419–2430, 2009, doi: 10.1016/j.watres.2009.02.039.

[43] P. Banerjee, P. Das, A. Zaman, and P. Das, "Application of graphene oxide nanoplatelets for adsorption of Ibuprofen from aqueous solutions: Evaluation of process kinetics and thermodynamics," *Process Safety and Environmental Protection*, vol. 101, pp. 45–53, May 2016, doi: 10.1016/j.psep.2016.01.021.

[44] M. Verma *et al.*, "Graphene oxide-manganese ferrite (GO-MnFe2O4) nanocomposite: One-pot hydrothermal synthesis and its use for adsorptive removal of Pb2+ ions from aqueous medium," *J Mol Liq*, vol. 315, Oct. 2020, doi: 10.1016/j.molliq.2020.113769.

[45] J. Ma, M. Yang, F. Yu, and J. Zheng, "Water-enhanced Removal of Ciprofloxacin from Water by Porous Graphene Hydrogel," *Sci Rep*, vol. 5, Sep. 2015, doi: 10.1038/srep13578.

[46] F. Wang, B. Yang, H. Wang, Q. Song, F. Tan, and Y. Cao, "Removal of ciprofloxacin from aqueous solution by a magnetic chitosan grafted graphene oxide composite," *J Mol Liq*, vol. 222, pp. 188–194, Oct. 2016, doi: 10.1016/j.molliq.2016.07.037.

[47] H. Mahmoodi, M. Fattahi, and M. Motevassel, "Graphene oxide-chitosan hydrogel for adsorptive removal of diclofenac from aqueous solution: preparation, characterization, kinetic and thermodynamic modelling.," *RSC Adv*, vol. 11, no. 57, pp. 36289–36304, Nov. 2021, doi: 10.1039/d1ra06069d.

[48] G. Wernke, Q. L. Shimabuku-Biadola, T. R. T. dos Santos, M. F. Silva, M. R. Fagundes-Klen, and R. Bergamasco, "Adsorption of cephalexin in aqueous media by graphene oxide: kinetics, isotherm, and thermodynamics," *Environmental Science and Pollution Research*, vol. 27, no. 5, pp. 4725–4736, Feb. 2020, doi: 10.1007/s11356-019-07146-y.

[49] A. Jaswal *et al.*, "Adsorptive removal of antibiotic ofloxacin in aqueous phase using rGO-MoS2 heterostructure," *J Hazard Mater*, vol. 417, Sep. 2021, doi: 10.1016/j.jhazmat.2021.125982.

[50] D. T. Ogunleye, S. O. Akpotu, and B. Moodley, "Crystalline Nanocellulose Anchored on Reduced Graphene Oxide for the Removal of Pharmaceuticals from Aqueous Systems: Adsorbent Characterization and Adsorption Performance," *ChemistrySelect*, vol. 8, no. 4, Jan. 2023, doi: 10.1002/slct.202202533.

[51] J. Yang, S. Shojaei, and S. Shojaei, "Removal of drug and dye from aqueous solutions by graphene oxide: Adsorption studies and chemometrics methods," *NPJ Clean Water*, vol. 5, no. 1, Dec. 2022, doi: 10.1038/s41545-022-00148-3.

[52] O. Moradi, H. Alizadeh, and S. Sedaghat, "Removal of pharmaceuticals (diclofenac and amoxicillin) by maltodextrin/reduced graphene and maltodextrin/reduced graphene/copper oxide nanocomposites," *Chemosphere*, vol. 299, p. 134435, Jul. 2022, doi: 10.1016/j.chemosphere.2022.134435.

[53] S. Bose and L. T. Drzal, "Role of thickness and intercalated water in the facile reduction of graphene oxide employing camera flash," *Nanotechnology*, vol. 25, no. 7, Feb. 2014, doi: 10.1088/0957-4484/25/7/075702.

[54] Z. Shahnavaz, P. M. Woi, and Y. Alias, "A hydrothermally prepared reduced graphene oxide-supported copper ferrite hybrid for glucose sensing," *Ceram Int*, vol. 41, no. 10, pp. 12710–12716, Jun. 2015, doi: 10.1016/j.ceramint.2015.06.103.

[55] T. Ramaprasad, R. J. Kumar, U. Naresh, M. Prakash, D. Kothandan, and K. C. B. Naidu, "Effect of pH value on structural and magnetic properties of CuFe2O4 nanoparticles synthesized by low temperature hydrothermal technique," *Mater Res Express*, vol. 5, no. 9, Sep. 2018, doi: 10.1088/2053-1591/aad860.

[56] R. S. Yadav *et al.*, "Structural, dielectric, electrical and magnetic properties of CuFe2O4 nanoparticles synthesized by honey mediated sol–gel combustion method and annealing effect," *Journal of Materials Science: Materials in Electronics*, vol. 28, no. 8, pp. 6245–6261, Apr. 2017, doi: 10.1007/s10854-016-6305-4.

[57] G. F. Goya, H. R. Rechenberg, and J. Z. Jiang, “Structural and magnetic properties of ball milled copper ferrite,” *J Appl Phys*, vol. 84, no. 2, pp. 1101–1108, Jul. 1998, doi: 10.1063/1.368109.

[58] D. Khalili, “Graphene oxide: a promising carbocatalyst for the regioselective thiocyanation of aromatic amines, phenols, anisols and enolizable ketones by hydrogen peroxide/KSCN in water.”

[59] E. Andrijanto, S. Shoelarta, G. Subiyanto, and S. Rifki, “Facile synthesis of graphene from graphite using ascorbic acid as reducing agent,” in *AIP Conference Proceedings*, American Institute of Physics Inc., Apr. 2016. doi: 10.1063/1.4945457.

[60] S. Jalili-Firoozinezhad *et al.*, “Polycaprolactone-templated reduced-graphene oxide liquid crystal nanofibers towards biomedical applications,” *RSC Adv*, vol. 7, no. 63, pp. 39628–39634, 2017, doi: 10.1039/c7ra06178a.

[61] A. C. Prabakar *et al.*, “Photocatalytic dye degradation properties of zinc copper ferrites nanoparticles,” *Journal of Nanostructures*, vol. 9, no. 4, pp. 694–701, Sep. 2019, doi: 10.22052/JNS.2019.04.011.

[62] N. K. Hejazy and T. M. Hammad, “Optical, Structural and Magnetic Properties of Copper-doped Iron Ferrite Synthesized by a Sol-Gel Method *,” 2019.

[63] L. K. Wu *et al.*, “Graphene oxide/CuFe2O4 foam as an efficient absorbent for arsenic removal from water,” *Chemical Engineering Journal*, vol. 334, pp. 1808–1819, Feb. 2018, doi: 10.1016/j.cej.2017.11.096.

[64] N. A. Khan *et al.*, “Efficient removal of norfloxacin by MOF@GO composite: isothermal, kinetic, statistical, and mechanistic study,” *Toxin Rev*, vol. 40, no. 4, pp. 915–927, 2021, doi: 10.1080/15569543.2020.1801750.

[65] F. Haghseresht and G. Q. Lu, “Adsorption characteristics of phenolic compounds onto coal-reject-derived adsorbents,” *Energy and Fuels*, vol. 12, no. 6, pp. 1100–1107, 1998, doi: 10.1021/ef9801165.

[66] W. Yang, Y. Lu, F. Zheng, X. Xue, N. Li, and D. Liu, “Adsorption behavior and mechanisms of norfloxacin onto porous resins and carbon nanotube,” *Chemical Engineering Journal*, vol. 179, pp. 112–118, Jan. 2012, doi: 10.1016/j.cej.2011.10.068.